Journal of Palaeosciences 71(2022): 19–43
0031–0174/2022

Depositional environments in the White Nile Valley during the last 300,000 years

MARTIN A.J. WILLIAMS[1,*], MICHAEL R. SNOW[2], PETER G. SELF[3], MARK D. RAVEN[3] AND E. JUN COWAN[4]

[1]*Earth Sciences, University of Adelaide, Adelaide SA 5005, Australia.*
[2]*South Australian Museum, Mineralogy Department, North Terrace, Adelaide SA 5000, Australia.*
[3]*CSIRO Mineral Resources, Waite Road, Urrbrae, Adelaide SA 5064, Australia.*
[4]*Earth, Atmosphere and Environment, Monash University, Clayton, Victoria 3168, Australia.*
[*]*Corresponding author: martin.williams@adelaide.edu.au*

(Received 16 December, 2021; revised version accepted 15 June, 2022)

ABSTRACT

Williams MAJ, Snow MR, Self PG, Raven MD & Cowan EJ 2022. Depositional environments in the White Nile Valley during the last 300,000 years. Journal of Palaeosciences 71(1): 19–43.

Before regulation, the White Nile contributed 83% of the low water flow to the main Nile and was responsible for maintaining the Nile as a perennial river during times of drought in Ethiopia. Two key unresolved questions relating to the White Nile are:

(a) When did the White Nile first join the main Nile?

(b) What type of sediment did the White Nile contribute to the main Nile?

The answer to the first question has important implications for our understanding of hydro–climatic and tectonic events in the Ugandan Lake Plateau. The answer to the second question is essential for correctly interpreting the sedimentary record preserved in the Nile deep sea fan in the eastern Mediterranean.

Our work has shown for the first time that the White Nile has been transporting smectite–rich sediments from the time of its probable inception over 240 ka ago and possibly since about 400 ka. Our analysis of the heavy mineral assemblages in White Nile alluvial sediments provides strong support for a source in the Lake Plateau region of Uganda. The White Nile was flowing from Uganda by at least 240 ka and very likely from about 400 ka.

Key–words—Nile, White Nile, Blue Nile, Clay Minerals, Heavy Minerals, Alluvial History, Nile Deep Sea Fan.

INTRODUCTION

THE Nile is the longest river in the world (6,953 km). It derives its water and sediment from two very different groups of tributaries–the Ugandan White Nile and the Ethiopian Blue Nile and Atbara (Woodward *et al.*, 2007, 2015, 2022; Padoan *et al.*, 2011; Garzanti *et al.*, 2015; Williams, 2019, 2021) (Fig. 1a). The White Nile rises in the equatorial uplands of Uganda and Rwanda (Fig. 1a) which are underlain by the Archaean Gneiss–Granulite Complex (Garzanti *et al.*, 2015, Fig. 10 and pp. 24–5), and flows from Lake Victoria through Lake Kyoga into Lake Albert (Fig.1a). It then flows across deeply weathered ancient metamorphic, igneous, and sedimentary rocks (Fig. 2), down a vast low angle alluvial fan into the Sudd swamps of South Sudan (Fig. 1a) and from there flows north to meet the Blue Nile at Khartoum (Fig.1a).

The headwaters of the Blue Nile flow down from the highly dissected Ethiopian Highlands into Lake Tana (Fig. 1b), which contributes only about 9% of the total Blue Nile discharge (Hurst, 1952). Below Lake Tana, the Blue Nile is entrenched in a very deep gorge which extends for about 350 km to the western edge of the Ethiopian escarpment. In places the gorge is 20–30 km wide at its summit and 1,500 m deep. In creating its gorge, the Blue Nile has cut down through Cenozoic basalts, Mesozoic and Palaeozoic sandstones, limestones, marls and gypsum down to the Precambrian basement rocks, all of which are clearly exposed in the gorge. The sides of the gorge are dissected by large tributaries which together provide the Blue Nile with most of its total water discharge and sediment load. The Blue Nile then emerges from the Ethiopian uplands and flows across the Gezira alluvial fan (Fig. 1c) to its confluence with the White Nile.

The Tekezze River rises to the north of the Blue Nile headwaters and is the major tributary of the Atbara. The Tekezze and Blue Nile gorges are two of the most impressive in Africa. McDougall *et al.* (1975) obtained the first potassium–argon ages (27–23 Ma) for the uppermost basalt flows in the gorge. They estimated that a total volume of rock

amounting to 100,000 ± 50,000 km^3 had been eroded from the two gorges from a combined upland drainage area of 275,000 km^2. The Blue Nile and Atbara rivers have been transporting sediments from the volcanic highlands of Ethiopia (Figs 1b, 2) to the eastern Mediterranean for at least thirty million years (Fielding *et al.*, 2016, 2018). Sediments in the White Nile are dominantly quartzose. Blue Nile and Atbara sediments are dominantly volcanic.

The Atbara and Blue Nile provide most of the present–day sediment load carried by the Nile during the months of

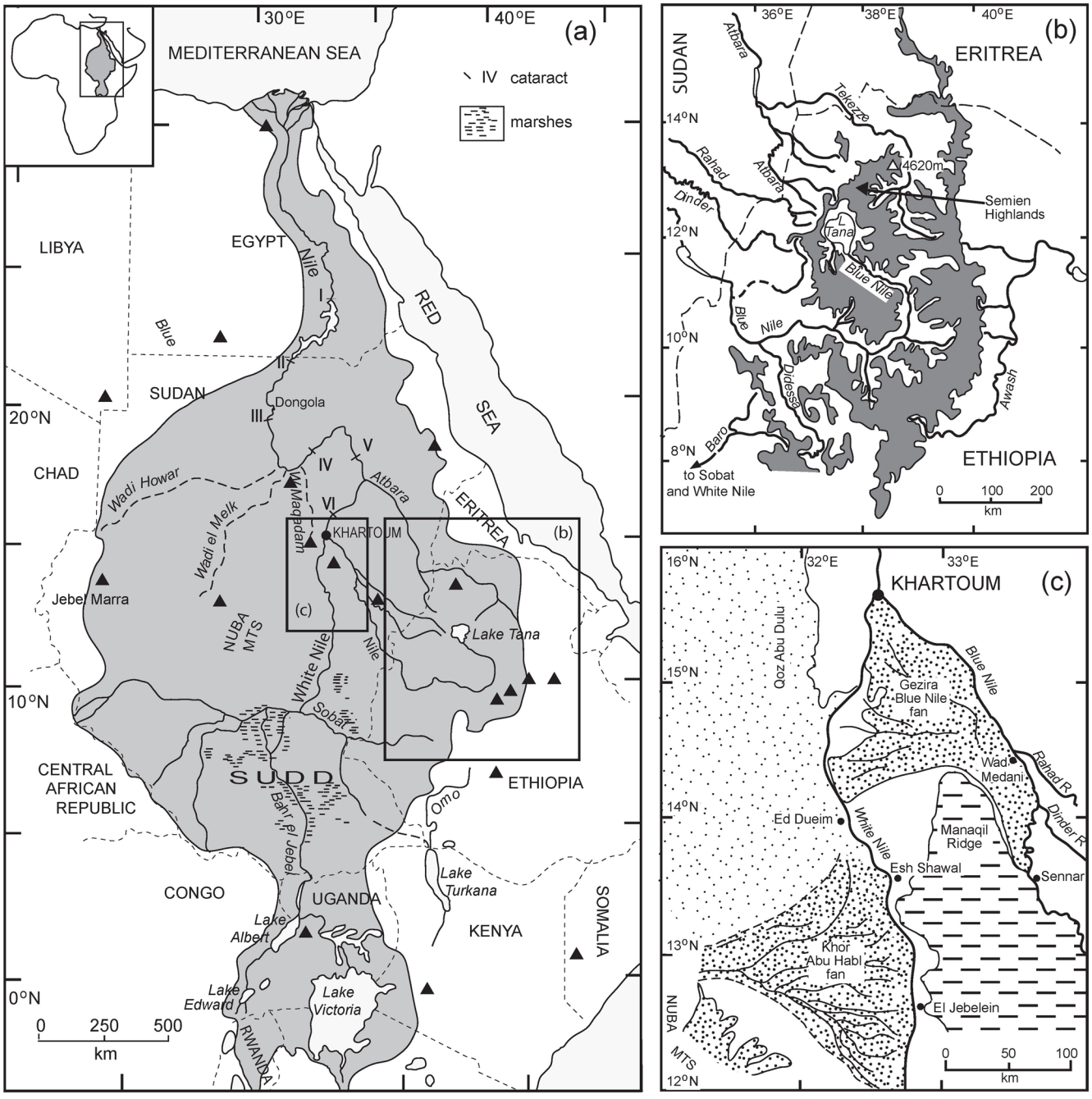

Fig. 1—(a) Map of the Nile Basin showing present–day watershed. Black triangles are localities investigated by the author in and near the Nile Basin. (b). Blue Nile headwaters. Dark shading represents land above 2 000 m elevation. Dashed lines show international boundaries. (c) The Gezira Blue Nile Fan and the Khor Abu Habl Fan (Adapted from Williams & Adamson, 1980, Fig. 12.6; Adamson *et al.*, 1982, Fig. 9.3; Williams, 2009, Fig. 3A; and Williams, 2019, Fig.11.1).

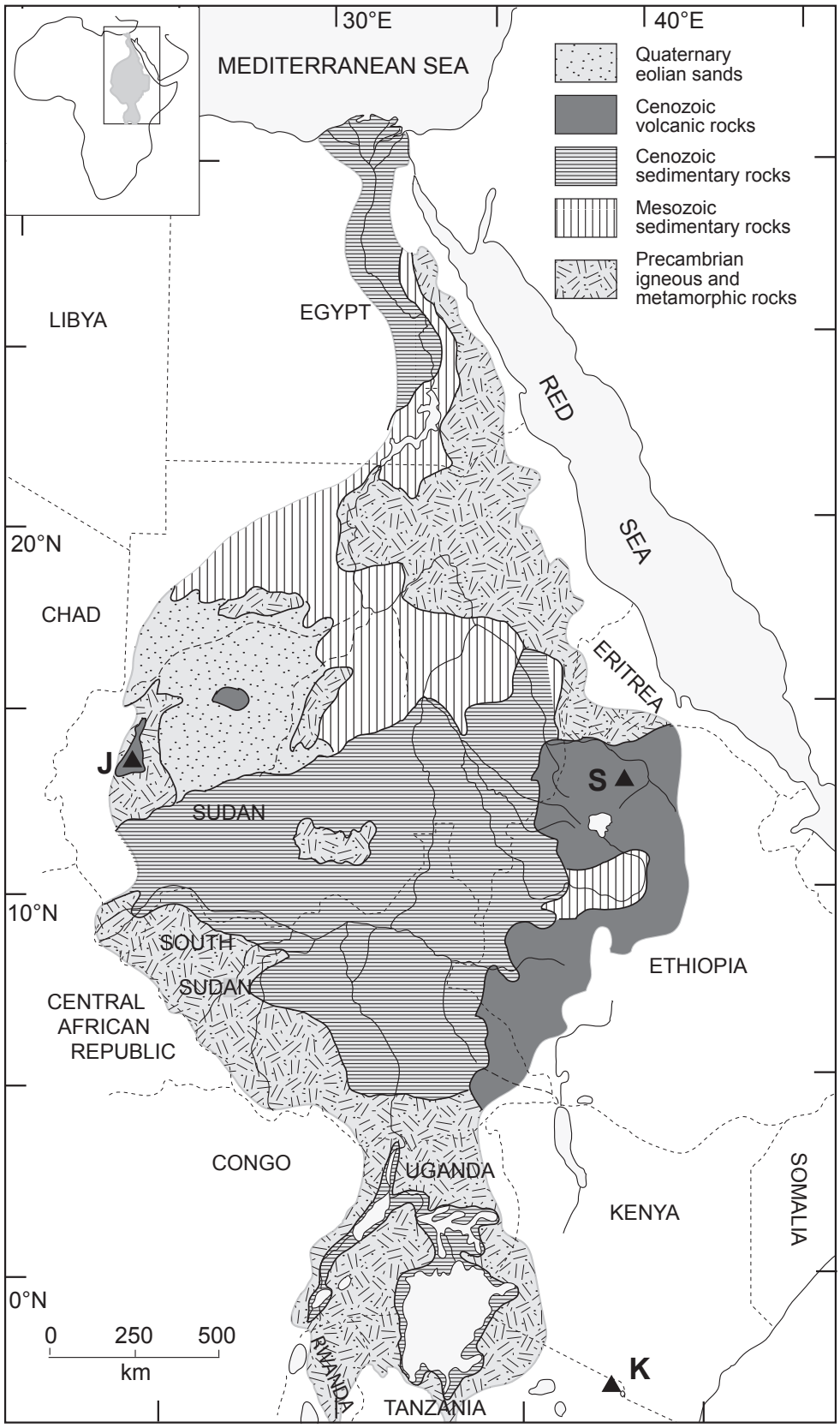

Fig. 2—Geology of the Nile Basin (After Williams, 2019, Fig. 4.3).

high flood discharge between June and September. A 3–year study by Omer el–Badri during 1967–69 showed that Blue Nile suspended sediment concentration at Khartoum was 100 mg/l in June and 4,000 mg/l in August, when discharge in that river is about twenty times more than in June (El Badri, 1972). Before regulation the White Nile contributed 83% of the low water flow to the main Nile (Table 1; Fig. 3). During dry years in the Ethiopian headwaters, it was the White Nile that maintained the main or Desert Nile as a perennial river. Without the White Nile, the Desert Nile would have had a very different and far more seasonal hydrological regime. On occasions when the Ugandan lakes dried out and flow in the White Nile ceased, such as during the Last Glacial Maximum some 20,000 years ago (Livingstone, 1980; Johnson *et al.*, 1996; Williams *et al.*, 2006; Stager & Johnson, 2008), the main Nile became a series of disconnected pools. These conditions had a profound impact upon the Upper Palaeolithic people living in the Nile Valley at that time (Vermeersch & Van Neer, 2015; Leplongeon *et al.*, 2020; Vermeersch, 2020; Williams, 2020).

CENOZOIC UPLIFT AND VOLCANISM

Arabia and Africa formed part of a single continent until the mid–Cenozoic opening of the Red Sea. Slow and prolonged crustal doming during the Oligocene created what Bowen and Jux (1987) termed the Afro–Arabian Dome. This elliptical dome was 1,500 km wide and 3,000 km long. It extended across Ethiopia and Yemen with its centre above the intensely hot Afar lithothermal plume in eastern Ethiopia (Avni *et al.*, 2012). Uplift of the dome caused sporadic reactivation of pre–existing fractures and shear zones. Many of these lineaments developed during the 550 Ma East African Orogenic events (Talbot & Williams, 2009; Fritz *et al.*, 2013) and some extend back well into the Precambrian. The angular pattern of the main Nile (Fig. 1a) reflects the structural control exerted by these features (Adamson & Williams, 1980; Adamson *et al.*, 1993). The uplift resulted in a long interval of regional denudation, lasting about 6–10 million years, during which a major erosion surface developed across the entire region. Avni *et al,* (2012) refer to this widespread erosion surface as the 'Oligocene regional truncation surface'. Uplift accelerated in the late Oligocene and early Miocene and rifts began to form by 25 Ma in what became the Red Sea and Gulf of Aden (Corti, 2009), disrupting the original Afro–Arabian lithospheric plate and leading to the formation of what became two separate plates–the African Plate and the Arabian Plate (Williams *et al.*, 2004). In Ethiopia uplift of what became the Ethiopian highlands was accompanied by widespread volcanic activity and the extrusion of numerous basalt flows. Hofmann *et al.* (1997) considered that most of these flood basalts were erupted within an interval of about one million years roughly 30 Ma ago.

Table 1—Present hydrological regime of the Nile (Adapted from Hurst, 1952; Williams *et al.*, 1982; Table 7.1).

River	Discharge (km^3)	Sediment load (10^6 t)	% of peak flow	% of low flow	Ratio of peak to low flow
White Nile	27.5	2	10	83	5: 2
Blue Nile	51	41	68	17	40: 1
Atbara	12.5	14	22	0	–
Main Nile	91	57			16: 1

TECTONIC HISTORY OF LAKE VICTORIA AND THE UGANDAN HEADWATERS OF THE WHITE NILE

Before the onset of rifting in Uganda and formation of the Western Rift, the rivers flowed westwards from the uplands in the east into the Congo/Zaïre Basin to the west. Rifting in the northern sector of the Western Rift began during the Miocene about 8–9 Ma ago (Talbot & Williams, 2009), and was accompanied by uplift along the rift margins. The rifting led to segmentation and diversion of the earlier drainage system (Talbot & Williams, 2009). Another result of the rifting was the formation of large lakes within the floor of the Western Rift, including Lake Albert (Fig. 1a). Another consequence of the earth movements associated with this rifting was the formation of Lake Victoria which now provides about 90% of the water that flows into the northern margin of lake Albert and from there into the White Nile. The age of Lake Victoria is poorly constrained. The maximum thickness of sediment within the lake amounts to only about 60 m (Johnson *et al.*, 1996). Extrapolating dated rates of Holocene and Late Pleistocene sedimentation gives an approximate age of 0.5 Ma for Lake Victoria (Johnson *et al.* 1996, Fig. 4).

AIMS OF THIS STUDY

The purpose of this study is to offer some provisional answers to two important but still unresolved questions relating to the White Nile. (a) When did the White Nile first join the main Nile? (b) What type of sediment did the White Nile contribute to the main Nile?

The answer to the first question has important implications for our understanding of hydro–climatic and tectonic events in the Ugandan Lake Plateau (Talbot & Williams, 2009; Williams & Talbot, 2009). The answer to the second question is essential for correctly interpreting the sedimentary record preserved in the Nile deep sea fan in the eastern Mediterranean (Williams, 2019, chapter 21).

Before attempting to answer these two questions, and to place them into context, we first discuss some puzzling features of the lower White Nile Valley. These features became particularly evident during soil surveys conducted east of the lower White Nile in the 1950s and 1960s (Sir Alexander Gibb & Partners, 1954; Hunting Technical Services Limited, 1964, 1965; Gunn, 1982; Williams *et al.*, 1982).

PUZZLING FEATURES OF THE LOWER WHITE NILE VALLEY

The lower White Nile is an enigmatic river. Perhaps its most puzzling attribute is its very low flood gradient of 1: 100,000 between Malakal and Khartoum (Fig. 4)–a fall of one centimetre per kilometre. This contrasts with the flood gradient of the Blue Nile, which amounts to 13 cm per kilometre between the Sudan–Ethiopia border and Khartoum. The remarkably low flood gradient of the White Nile has generated a great deal of speculation, with the most persistent theme being that the river is flowing over the bed of a former lake (Lombardini, 1864, 1865), which we discuss in the next section.

Another curious feature of the White Nile is its relatively straight channel pattern, despite its gentle gradient and fine suspension load, two attributes usually associated with highly sinuous meandering river channels. The channel pattern in the lower White Nile Valley is braided, with channels diverging around islands of varying size (Fig. 4). The larger of these islands are composite features consisting of a series of very large juxtaposed mid–channel bars several kilometres in length.

Once they became exposed to subaerial weathering processes and plant growth, the terminal Pleistocene–Holocene alluvial clays of the White Nile were converted by soil–forming processes into dark grey–brown cracking clays, or *vertisols*, which are on average about 1.0–1.5 m thick. Beneath the vertisols in some places there are sporadic shell beds which extend up to 11 km east of the present river and up to 4 m above the modern unregulated mean maximum flood level of the White Nile.

The subsoils close to and east of the present White Nile are locally very saline. Elsewhere they consist of highly localized concentrations of micro–crystalline calcite and dolomite.

North of about latitude 13°35′N the dark cracking clays abut against quartz sand dunes. Linear and parabolic dunes are common along the lower reaches of the White Nile north of latitude 14°10′N.

From about the latitude of Melut northwards (Fig. 5) there are two very distinct breaks of slope in the otherwise gently sloping land bordering the White Nile flood plain. These steeper sectors occur at elevations of 382 m and 386 m above the Alexandria mean sea level height datum.

Questions relating to these enigmatic features in the lower White Nile Valley include:

1. Why is the flood gradient so low?

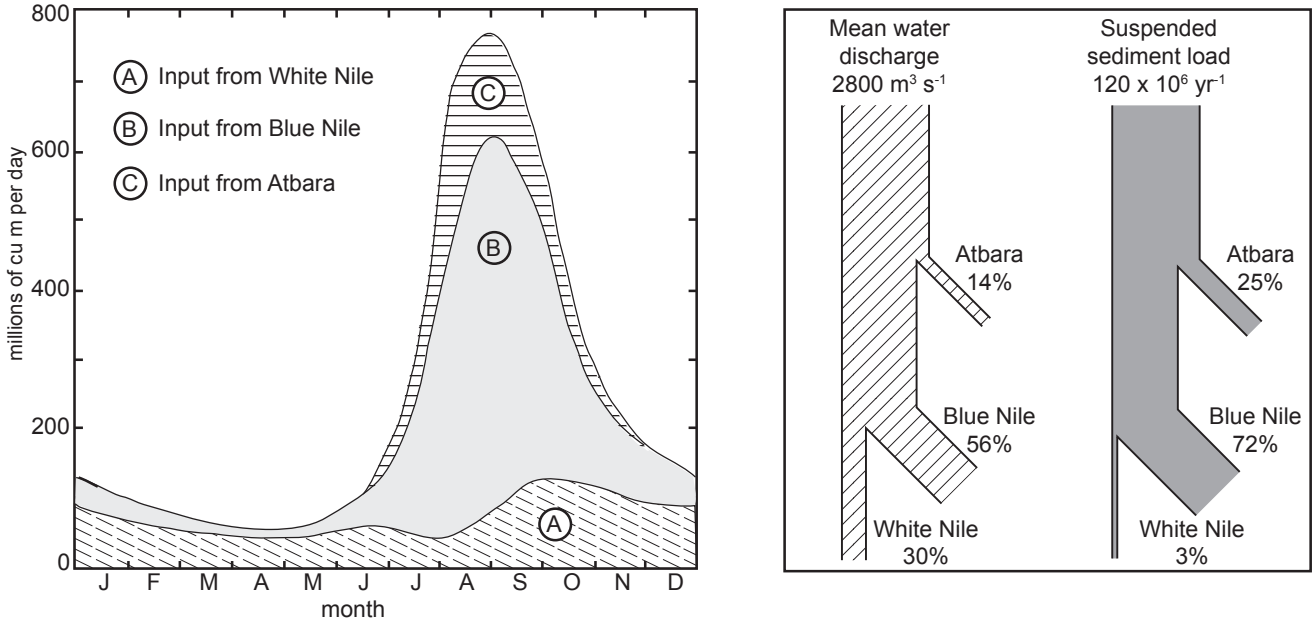

Fig. 3—(a) Mean monthly discharge of the Blue Nile, the White Nile and the river Atbara, and total discharge for the main Nile, based on 1912–1936 averages. (After Hurst, 1952, Fig. 16). (b) Mean annual suspended sediment loads and discharge for the Blue Nile, the Atbara and the White Nile (After Woodward *et al.*, 2007, Fig. 13.11).

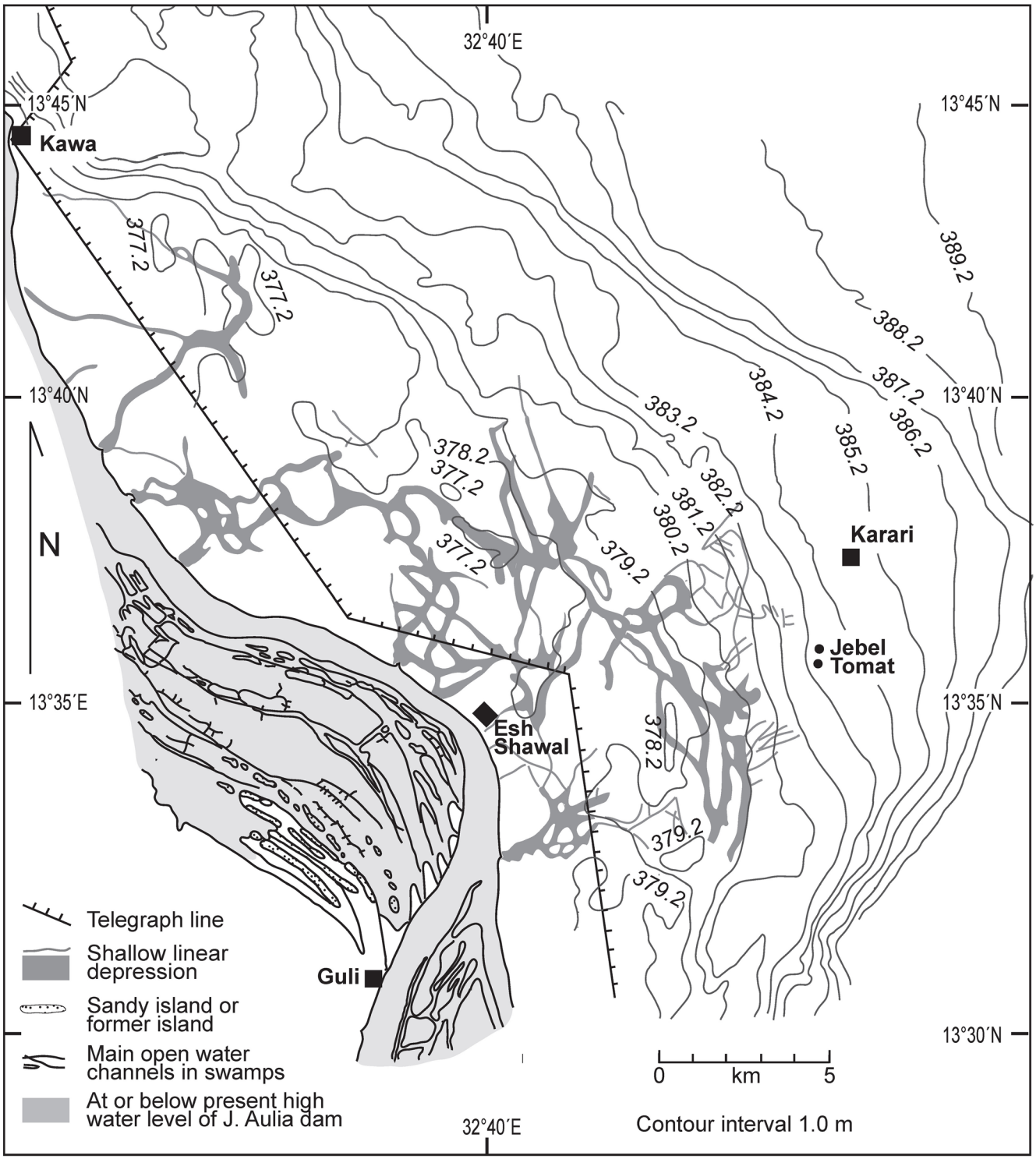

Fig. 4—Drainage channels on the Holocene floodplain east of the present White Nile in the vicinity of Esh Shawal (After Williams, 2009, Fig. 7A).

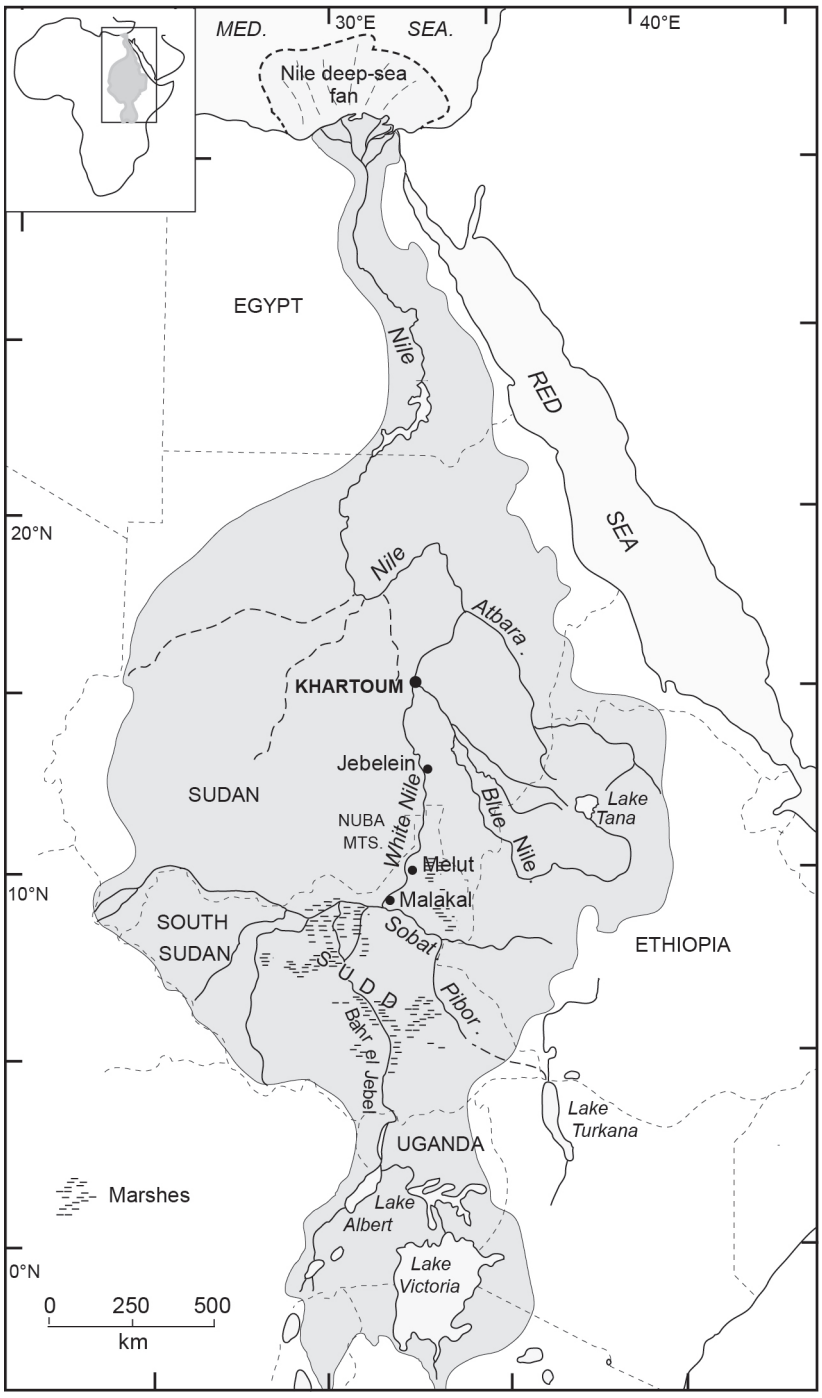

Fig. 5—Map of the Nile Basin showing places cited in the text.

2. Does the White Nile flow across the bed of a former lake?
3. What do the buried shell beds denote? Do they represent former flood levels, or beach debris, or the channel bed?
4. What do the 382 m and 386 m breaks of slope indicate?
5. Why are some subsoils highly saline?
6. What is the relationship between the sand dunes and the White Nile alluvium?
7. How did the micro–crystalline carbonates form? Are they saline? Did they form during or after deposition of the sediments in which they occur?

Any coherent and convincing reconstruction of the Quaternary alluvial history of the White Nile needs to account for each of the puzzling features described above.

PUZZLING FEATURES OF THE LOWER WHITE NILE VALLEY EXPLAINED

Over a century ago, the eminent hydraulic engineer Sir William Willcocks pointed out that during the height of the Blue Nile floods, when the discharge in that river amounted to 11,000 cubic metres a second, flow in the White Nile was impeded, causing the White Nile to form a lake fed by the Blue Nile flood waters that extended up to 300 km upstream of the Blue Nile–White Nile confluence at Khartoum. Once Blue Nile discharge fell to about 6,000 cubic metres a second, the impounded waters of the White Nile were released into the main Nile (Willcocks, 1904). This shallow seasonal lake provides a good analogue for what happened at intervals in the late Quaternary during periods of unusually high flood discharge in the Blue Nile. The two most recent times when this occurred were during the Last Interglacial about 125,000 years ago (125 ka) and during the abrupt return of the summer monsoon 14,500 years ago (14.5 ka) (Talbot *et al.*, 2000; Williams *et al.* 2006). The 386 m break of slope marks the highest point reached by the seasonal White Nile Lake during the Last Interglacial (Fig. 6) until it finally receded from about 110 ka onwards. Barrows *et al.* (2014) used the cosmogenic isotope ^{10}Be to date the 386 m sandy shoreline near Jebelein (Fig. 6).

The 382 m break of slope represents the maximum height reached by the terminal Pleistocene seasonal White Nile Lake about 14.5 ka ago (Fig. 7). Over seventy years ago J.D. Tothill discovered remains of a former shoreline at an elevation of 382.14 m on the dune behind the Inspector's house at Hashaba (Fig. 7) with water worn shells of *Cleopatra* and *Melanoides* which he considered to be 'dead adults washed up from the river or lake bed by wave action' (Tothill, 1948, p. 134). He concluded that the Hashaba dunes were not true desert dunes but were the remains of lakeside dunes, and that 'this strandline probably marks the winter shoreline of this lake at the time of its greatest development' (op. cit., p. 134). We concur with Tothill that 382.14 m was the highest level attained by the terminal Pleistocene White Nile Lake (had it been higher the fragile shells would have been destroyed) but we consider that it was a summer and not a winter shoreline. Sadly, the site had already been obliterated by the passage of camels, donkeys, and humans by the time one of us (MAJW) visited this locality in November 1963.

As the lake receded progressively it left a layer of dead aquatic snails which now form a shell bed about 10 cm thick. This shell bed was subsequently buried beneath the Holocene flood plain clays of the White Nile. Sporadic concentrations of aquatic snail shells at lower elevations indicate times of high Holocene flood levels in the White Nile (Williams, 2009). As the receding 382 m lake dried some water was left behind in broad shallow depressions (Fig. 4) known locally as *maya'as*. As the water in the depressions evaporated it became increasingly saline, as did the sediments on the floor

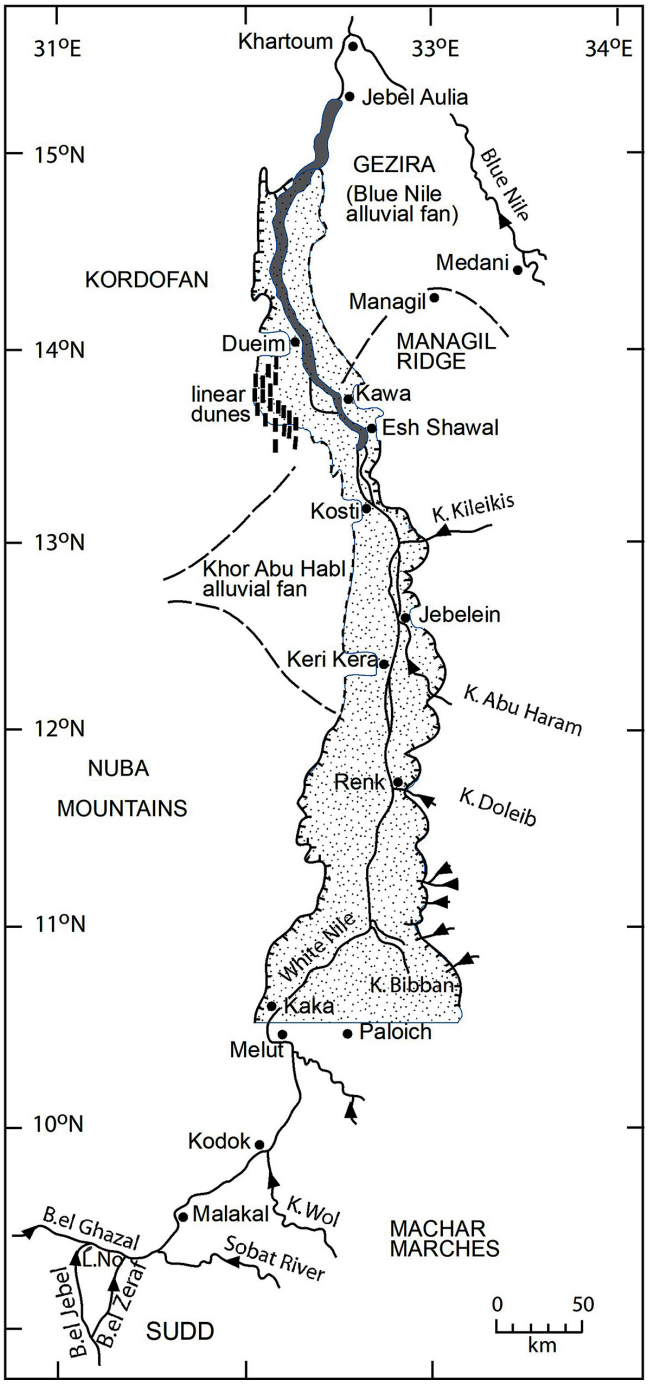

Fig. 6—The Last Interglacial White Nile Lake (After Williams *et al.*, 2003, Fig. 1 and Williams, 2009, Fig. 2).

of the depressions. These highly saline sediments were later buried beneath non–saline and non–alkaline flood plain clays, but their presence in the subsoil remains a hazard for present–day agriculture (Williams, 1968). This summary answers questions 1 to 5.

The origin of the sand dunes (question 6 in the preceding section) that occupy about 160,000 ha east of the lower White Nile and extend for over 100 km between 14°15′N and 15°15′N is also unusual in that they derive from sandy sediments transported across the Gezira alluvial fan by ancient distributary channels of the Blue Nile (Fig. 8). The Gezira lies between the lower Blue and White Nile rivers and is bounded to the south by the Managil Ridge (Fig. 1c) and is a very large low angle alluvial fan built up by the Blue Nile since its inception some 30 million years ago (McDougall *et al.*, 1975). These abandoned Blue Nile channels were first recorded by Williams (1966) and later mapped from 1: 25,000 scale air photos and 1: 50,000 scale topographic maps with contours at 50 cm intervals (Adamson *et al.*, 1982, p. 176, Fig. 9.3; Williams, 2009, Fig. 3A) but it was not until just over a decade ago that optically stimulated luminescence (OSL) and radiocarbon (^{14}C) ages were finally obtained for some of these ancient channels (Williams *et al.*, 2010, 2015). The dated channels were actively transporting alluvial sands between 100 ka and 70 ka. Clay was accumulating in backswamps near the channels between 70 ka and 50 ka, and the channels finally became defunct between 12 ka and 5 ka, most probably because of incision by the Blue Nile during the early to mid–Holocene (Adamson *et al.*, 1982, pp.186–9; Williams, 2019, pp.153–4).

In their distal reaches the alluvial sands ferried in by the former Blue Nile channels were blown out of the channels during the dry season to form source–bordering dunes. For a source–bordering dune to form there are three prerequisites: a regular seasonal replenishment of the channel sands, sparse riparian vegetation, and strong unidirectional winds during the dry season. Such dunes are indicative of a semi–arid rather than an arid climate. A pilot study of the heavy minerals collected from six dune sites on a 100 km N–S transect east of the lower White Nile at depths of 1.0. 2.0 and 2.7 m revealed that the heavy mineral assemblage was similar to that obtained from a sample of channel sand collected by MAJW in December 1971 from the Blue Nile gorge in Ethiopia (Williams & Adamson, 1973). The dunes have OSL ages of 115–105 ka, 60 ka and 12–7 ka and in places overlie the distal reaches of the former Blue Nile channels (Williams *et al.*, 2015). Close to the river the margins of many dunes show evidence of erosion during times of high White Nile floods (Williams, 2009, Fig. 4).

We discuss the age and origin of the microcrystalline calcite and dolomite (question 7) in the next section.

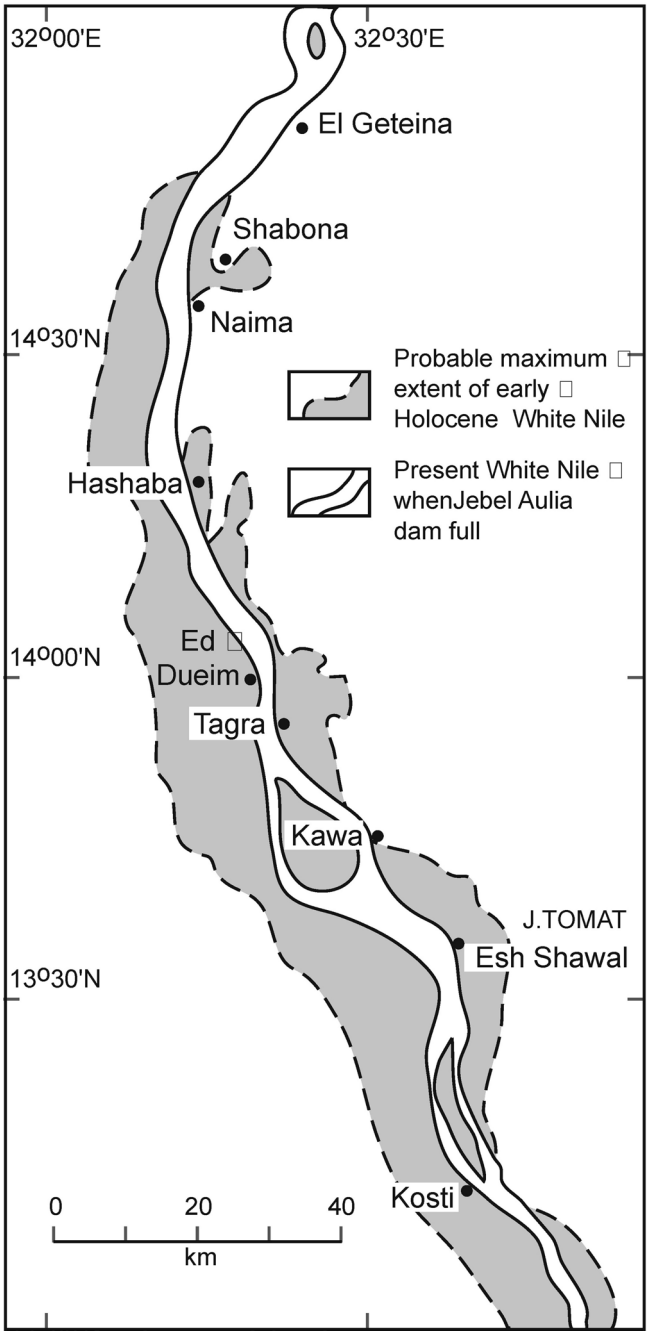

Fig. 7—Approximate extent of the terminal Pleistocene 382 m White Nile Lake (Adapted from Adamson *et al.*, 1982, Fig. 9.11).

ALLUVIAL STRATIGRAPHY IN THE LOWER WHITE NILE VALLEY

Mapping and sampling the soils east of the lower White Nile between Kosti and Khartoum during 1963–4 by one of us (MAJW) was based on 441 boreholes and 126 soil pits dug to a minimum depth of 2 metres (Hunting Technical Services Limited, 1965, p. 38). This was followed in the 1970s by a programme of systematic sampling and ^{14}C dating of shell and other samples obtained from over fifty additional boreholes and soil pits. These surveys suggested that the area immediately east of Esh Shawal (Fig. 9a), warranted more detailed study.

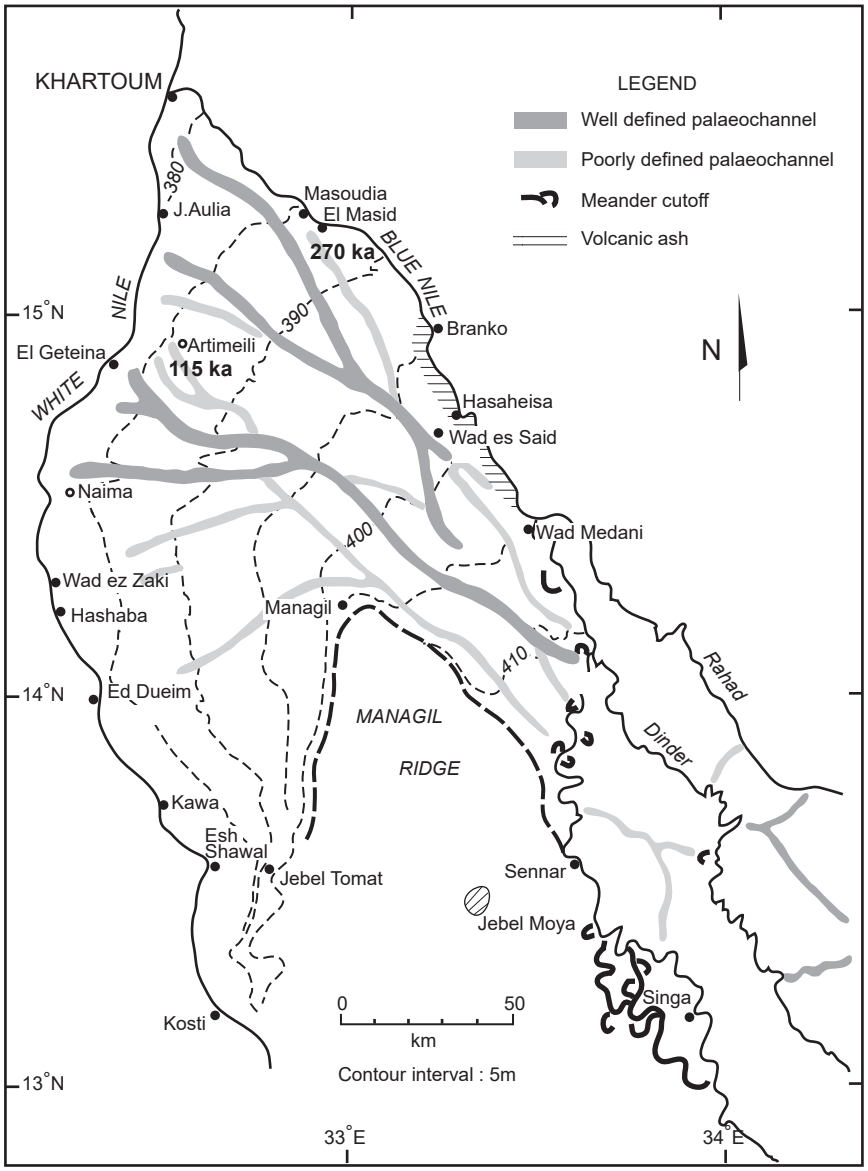

Fig. 8—Late Pleistocene and Holocene Blue Nile palaeochannels (Adapted from Adamson *et al.*, 1982, Fig. 9.3 and Williams, 2009, Fig. 3A).

A levelled transect running east from Esh Shawal for 11 km to the two granitic Basement Complex hills known locally as Jebel Tomat proved informative (Fig. 9b). Boreholes and soil trenches revealed that a surface unit of dark grey–brown clay up to 1.5–2.0 m thick was underlain by a shell breccia layer 10–15 cm thick which rose gradually eastwards to a maximum elevation of about 382 m. The sub–fossil shells included the aquatic snail species *Cleopatra bulimoides, Corbicula fluminensis, Biomphalaria pfeifferi* and *Melanoides tuberculata, Lymnaea natalensis* and *Bulinus truncatus,* and the Nile oyster *Etheria elliptica.* The shells have calibrated ^{14}C ages between 14.7 and 13.1 ka and accumulated during the time of the 382 m seasonal White Nile Lake discussed earlier. Beneath the shell breccia was an olive sandy clay or sandy clay loam up to 2 m thick which was in turn underlain by a well–sorted pale yellow quartz sand up to 1 m thick. The sand was in turn underlain by carbonate evaporite deposits up to 1 m thick. The lowest unit revealed in some of the deeper boreholes was an olive clay with traces of very fine horizontal bedding which extended 2 km east of Jebel Tomat to a maximum elevation of about 386 m.

Chemical analysis supplemented by scanning electron microscope photographs (Adamson *et al.*, 1982, Fig. 9.10) demonstrated that the fine carbonate sampled in two soil trenches dug in January 1973 consisted of microcrystalline high magnesian calcite at a depth of 3.8 m in trench ES1 (13°35'20"N; 32°40´E) and of a mixture of microcrystalline high magnesian calcite and dolomite crystals at a depth of

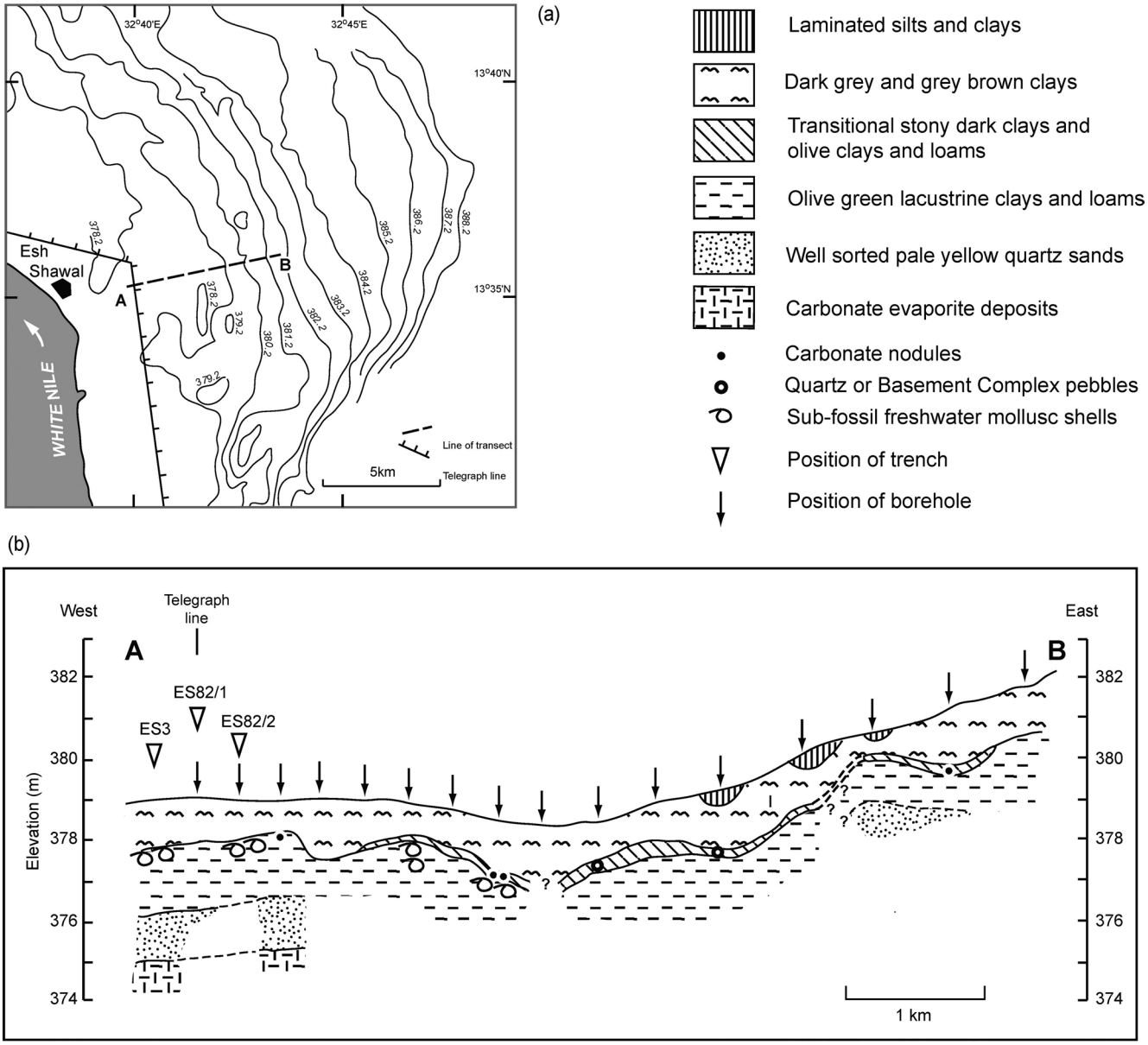

Fig. 9—(a) Location of transect AB. (b) 11 km long stratigraphic transect between Esh Shawal and Jebel Tomat, lower White Nile Valley (Adapted from Adamson *et al.*, 1982, Fig. 9.16; and Williams, 2019, Fig. 8.3B).

410 cm in trench ES3 which was located 1 km west of trench ES1. The ^{14}C ages obtained for these evaporite minerals had relatively large error terms but were consistent with late Pleistocene desiccation along the White Nile (Williams & Adamson, 1974).

Recent work by Caroline Mather provides a valuable insight into how the dolomite may have formed. Mather (2020) investigated dolomite precipitation in shallow groundwater in the semi–arid Hamersley basin of northwest Western Australia. She found that smectite minerals and microbial extracellular polymeric substances (EPS) provided a substrate for dolomite nucleation and growth. Dolomite precipitation was associated with evaporation and carbon dioxide degassing from shallow alkaline groundwater rich in magnesium derived from weathering of marine dolomitic basement rocks. It seems highly likely that similar processes were operating at shallow depth within the alluvial sediments of the lower White Nile during arid climatic intervals in the late Quaternary.

On the eastern edge of the pediment between the two granite hills of Jebel Tomat the dark grey–brown cracking clay is overlain by 60–80 cm of surface colluvium at 13°36' N, 32°44'30" E. At the contact between dark clay and colluvium a well–preserved *Limicolaria flammata* shell had

a calibrated ^{14}C age of 5,160 ± 206 (Williams, 2009, Table 1). *Limicolaria flammata* is a large land snail that is common today in the acacia–tall grass savanna plains south of Sennar (Fig. 1c) where the mean annual precipitation ranges between 400 and 800 mm. Its presence at the Jebel Tomat site shows that flooding from the White Nile up to that elevation had ceased by about 5,000 years ago at a time when the mean annual rainfall was up to twice that of today. The progressive increase in the percentage of the land snail *Limicolaria* in the upper 140 cm of the Gezira clay and the sharp decrease in the percentage of the aquatic snail *Cleopatra* between 160 and 50 cm depth is consistent with progressive desiccation of the Gezira during the early to mid–Holocene (Tothill, 1946; Williams, 2019, Fig. 11.2).

Stratigraphy of Esh Shawal trench ES82/1

It soon became clear that an independent dating method–optically stimulated luminescence or OSL–was needed to determine the age of the deeper sediments that were beyond the range of ^{14}C dating. Accordingly, two undisturbed White Nile sediment cores or monoliths were collected on October 29, 1982, from the southern face of trench ES82/1 near the village of Esh Shawal on the east bank of the White Nile at 13°35′N, 32°41′E. The trench was 6 m deep. The lower core was 0.7 to 1.7 m from the base and 5.3 to 4.3 m from the surface. The upper core was 4.35 to 4.85 m from the base and 1.65 to 1.15 m from the surface (Fig. 10). The grain size in each core was analysed at 10 cm intervals (Fig. 11; Table 2). Dispersed samples of clay and silt were determined using the pipette method and the sand fraction sieved, dried and weighed (USDA, 1996). A square section 5 x 5 cm rigid plastic gutter tray was placed vertically against the face of the trench. A steel chisel was used to carve the sediment and insert the tray carefully around the soil monolith. The tray containing the monolith was removed and wrapped in thick sheets of opaque plastic so that the monolith was not exposed to light. Bulk samples were then collected from each main stratigraphic unit from the base upwards to avoid any contamination from younger sediment. Fig. 10 shows the 8 main stratigraphic units numbered from the base up and the location of the two monoliths. A brief description follows. The 1982 provisional field interpretations of the beds are shown in brackets. All colours are moist Munsell Soil Colour Chart colours.

Bed 1: 0–105 cm (bottom of pit) 7.5Y5/2 dark olive green very fine sandy clay, fissile, fine horizontal laminations, massive, slickensides, swelling and cracking clay, along cracks 20–25% carbonate (hard to friable, not strongly cemented); up to 50% olive yellow sandy clay thrust into and against olive clay (i.e., a clay, sandy clay, carbonate breccia); pockets 5–10 cm diameter of sandy clay with > 50% carbonate (The olive clay is the primary deposit and increases with depth. The disturbed upper portion of this bed consists of roughly equal proportions of olive clay, yellow sandy clay, and carbonate. The green colour and fine laminations suggest that the primary sediment is lacustrine). Gradational irregular contact to:

Bed 2: 105–200 cm 5Y7/2 very pale olive yellow clayey fine, medium, and coarse sand, massive, traces of horizontal/sub–horizontal bedding, sporadic 0.5 to 2 cm rip–off clasts of dark olive clay derived from Bed 1; contact with Bed 3 undulating through 5 cm across 2 m. Sporadic concentric grey–brown sandy clay mudballs 5–15 cm diameter. West

Table 2—(a) Grain size data for the upper core (ES82U) shown on Fig. 10. (b) Grain size data for the lower core (ES82L) shown on Fig. 10. (c) Grain size data from the upper and lower cores shown on Fig. 10 related to depth from the surface and the stratigraphic bed number.

ES82U	**0 cm %**	**10 cm %**	**20 cm %**	**30 cm %**	**40 cm %**	**50 cm %**
< 2 µm	56.5	49.7	23.2	48.7	50.6	47.6
2–3.9 µm	4.8	6.2	1.1	3.6	3.6	5.8
3.9–7.8 µm	3.5	6.0	1.7	2.8	3.1	4.4
7.8–15.6 µm	4.3	6.4	1.7	1.3	2.1	3.2
15.6–31.2 µm	8.0	7.1	2.8	2.1	2.4	2.8
31.2–62.5 µm	8.0	5.7	1.8	2.6	3.0	3.6
62.5–125 µm	5.2	5.2	15.0	13.7	12.3	9.4
125–250 µm	5.2	5.2	29.4	17.6	15.4	14.1
250–500 µm	2.1	2.4	10.2	5.5	4.6	5.1
500–1000 µm	1.1	1.7	5.0	1.7	2.1	2.4
> 1000 µm	0.3	3.0	8.6	1.2	1.1	2.1
Total %	**98.9**	**98.7**	**100.4**	**100.8**	**100.3**	**100.5**

(a)

ES82L	**0 cm %**	**10 cm %**	**20 cm %**	**30 cm %**	**40 cm %**	**50 cm %**	**60 cm %**	**70 cm %**	**80 cm %**	**90 cm %**
< 2 μm	8.2	8.5	10.7	18.0	28.8	17.1	12.9	15.1	28.4	33.3
2–3.9 μm	0.2	0.5	1.8	1.9	1.7	2.8	2.4	1.4	3.1	4.3
3.9–7.8 μm	0.4	0.9	5.5	3.7	2.5	7.8	4.4	2.4	4.8	4.8
7.8–15.6 μm	0.4	2.1	8.0	1.5	1.4	7.0	2.4	1.2	2.5	2.9
15.6–31.2 μm	0.0	1.1	2.0	0.6	2.3	1.7	0.5	0.5	1.2	1.6
31.2–62.5 μm	0.4	1.9	1.9	1.3	2.9	2.8	1.1	1.4	2.2	2.8
62.5–125 μm	18.7	19.4	13.6	19.2	15.2	17.5	25.7	25.7	20.8	12.9
125–250 μm	53.5	44.0	32.6	41.9	33.9	24.1	40.1	41.3	23.4	15.0
250–500 μm	10.9	10.5	9.6	7.6	8.4	6.5	6.0	5.5	3.5	5.2
500–1000 μm	4.9	6.0	6.2	2.9	2.1	5.1	3.5	2.7	3.4	4.3
>1000 μm	1.6	4.3	6.0	2.4	0.5	6.5	1.1	2.2	6.4	13.2
Total %	**99.2**	**99.3**	**98.0**	**100.9**	**99.7**	**98.8**	**100.1**	**99.6**	**99.8**	**100.4**

(b)

Distance below top of upper core ES82U	**Depth from top of trench (cm)**	**Stratigraphic bed number**	**Comment**
0 cm	115	8	Holocene vertisol
10 cm	125	8	Holocene vertisol
20 cm	135	7	14.5 ka shell bed
30 cm	145	6 (top)	Olive fine sandy clay loam
40 cm	155	6	Olive fine sandy clay loam
50 cm	165	6	Olive fine sandy clay loam
Distance below top of lower core ES82L			
0 cm	430	2	Olive yellow clayey fine sand
10 cm	440	2	Olive yellow clayey fine sand
20 cm	450	2	Olive yellow clayey fine sand
30 cm	460	2	Olive yellow clayey fine sand
40 cm	470	2	Olive yellow clayey fine sand
50 cm	480	2	Olive yellow clayey fine sand
60 cm	490	2 (base)	Olive yellow clayey fine sand
70 cm	500	1	Dark olive clay with fine sand
80 cm	510	1	Dark olive clay with fine sand
90 cm	520	1	Dark olive clay with fine sand

(c)

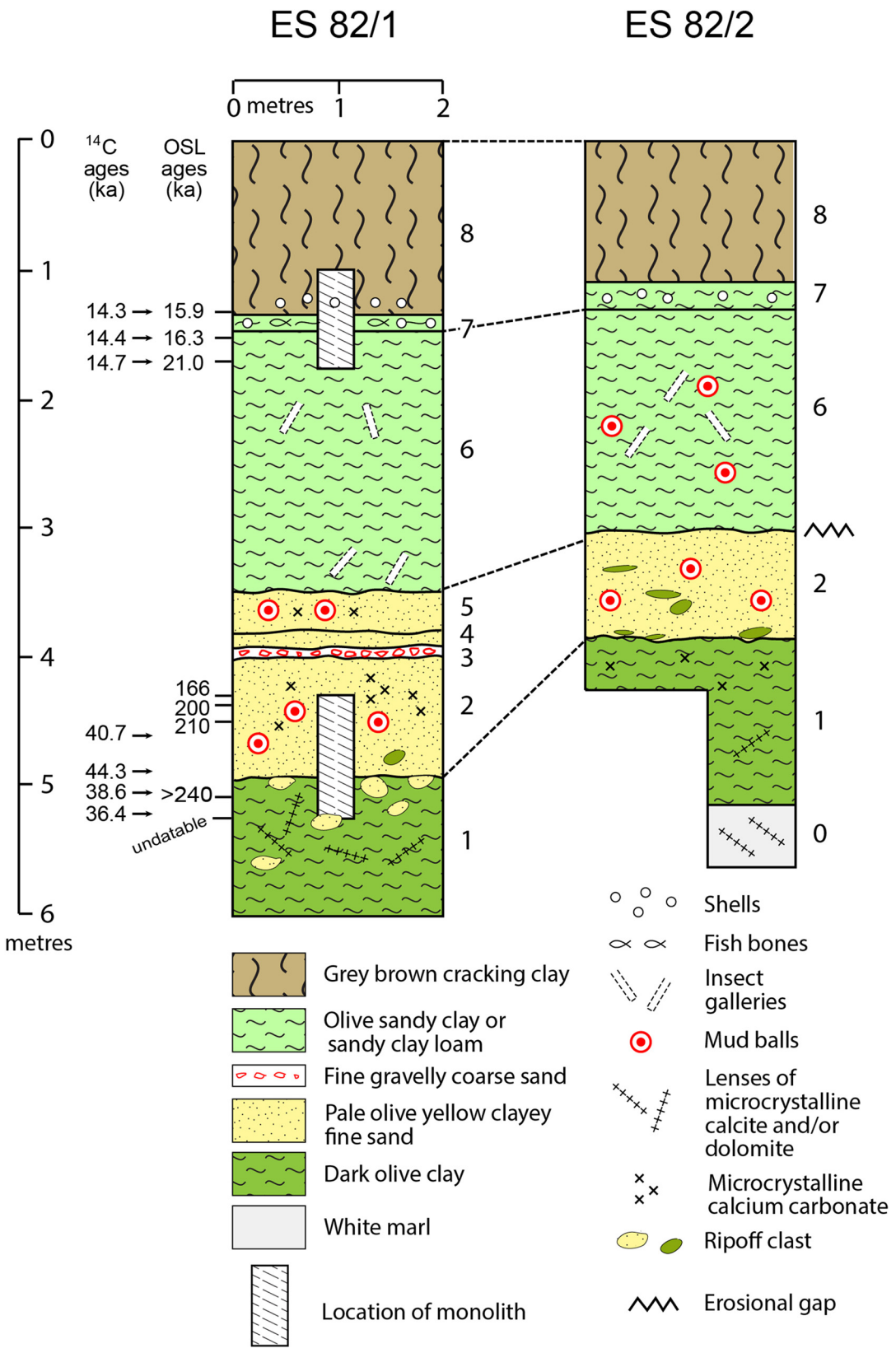

Fig. 10—Stratigraphic section of White Nile alluvium revealed in trenches ES82/1 and ES82/2. The error terms for the samples dated by OSL and ^{14}C are given in Tables 3 and 4.

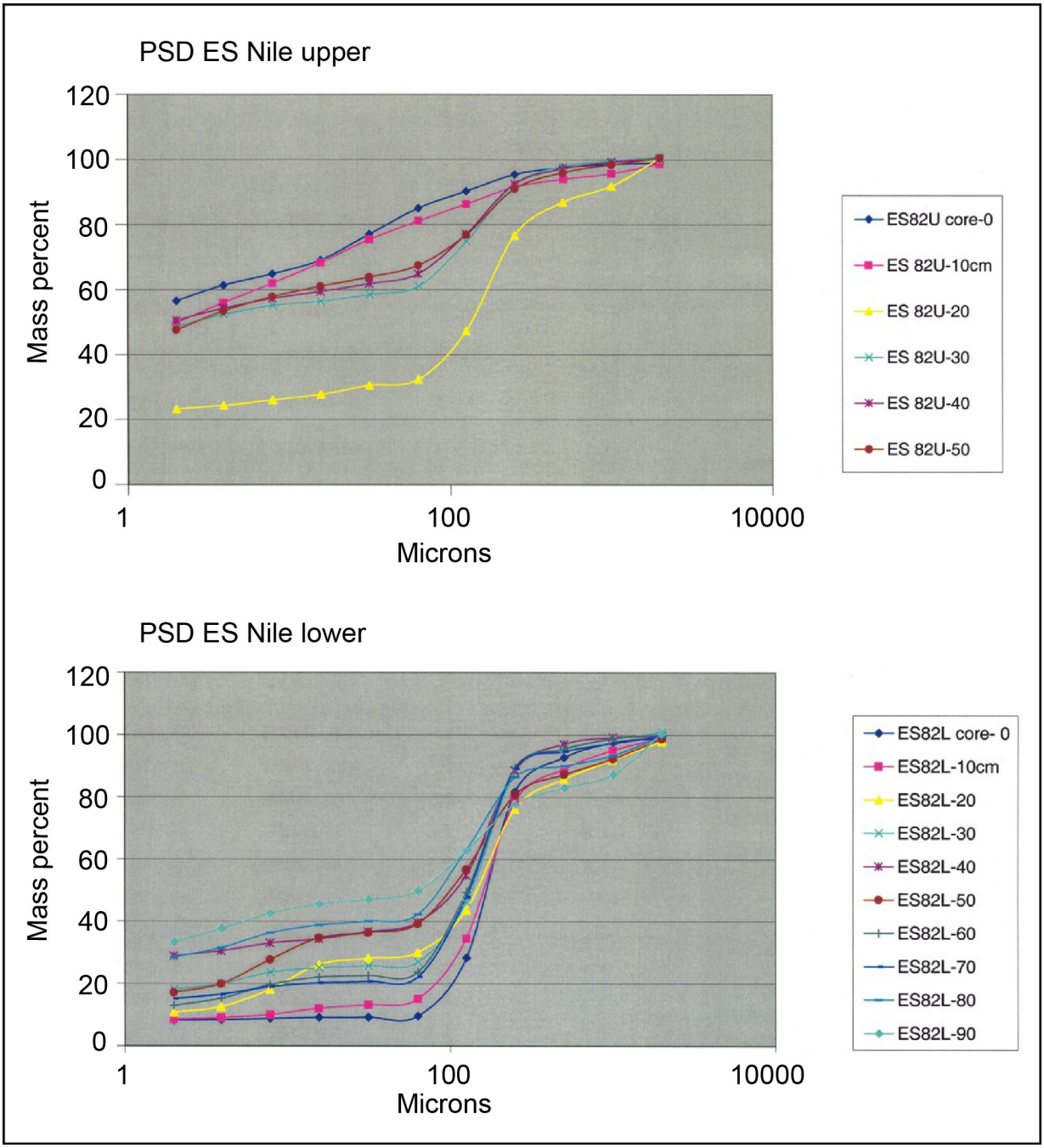

Fig. 11—Cumulative curves of particle size analysed at 10 cm intervals in the upper and lower cores/monoliths shown on Fig. 10.

face at 140–155 cm grey–brown sandy clay clasts 25 cm long, 15 cm high in yellow clayey sand matrix. Similar mudballs in bed 4. Mudballs start at 120 cm and occur up to 250 cm. >15% carbonate (Fluviatile).

Bed 3: 200–210 cm 2.5Y7/3 pale yellow coarse sandy matrix of gravel band 5–10 cm thick in south face. Fine gravelly coarse sand. Gravel 0.5 to 1.0 cm quartz (provenance probably local Basement Complex rocks which form the two low granitic hills of Jebel Tomat located 11 km to the east) with some rolled hard 1.0 cm carbonate concretions. Proportion of gravel to matrix drops in north face to 5–10% 0.3 cm sub–angular quartz; occasional platy quartz flakes up to 3 cm (artefacts?). Gravel matrix varies from olive sandy clay in south face to yellow clayey sand in north face. Gravel

Table 3—OSL ages of White Nile alluvium collected from trench ES82/1.

Sample no.	Depth (cm)	Bed	Age (ka)
ES82/1.3	130	8	15.9 ± 2.3
ES82/1.5	150	6	16.3 ± 2.2
ES82/1.7	170	6	21.0 ± 2.6
ES82/4.3	430	2	166 ± 30
ES82/4.35	435	2	200 ± 41
ES82/4.5	450	2	210 ± 30
ES82/5.1	510	1	> 240 ka
ES82/5.3	530	1	undatable

iron–stained to 7.5YR/4/4 pale reddish–brown in lower 4–5 cm of south face; upper 5 cm grey and iron–depleted (Local sheet floods during time of low White Nile).

Bed 4: 210–215/220 cm 7.5Y5/2 olive green slightly calcareous very fine sandy clay; slightly pedal, overlying the sheet flood gravel band (Fluviatile, some dust input).

Bed 5: 220–250 cm olive yellow massive calcareous clayey fine sand, very similar to bed 2. Scattered friable carbonate (Fluviatile followed by desiccation).

Bed 6: 250–455 cm with a weak moderate prismatic structure, base 7.5Y6/2 pale grey–brown to olive very fine sandy clay, weak fine vertical and oblique cracks; grades upwards progressively into 5Y5/2 olive very fine sandy clay with weak fine vertical cracks, otherwise massive; 10–20% carbonate Insect galleries in lower 150 cm. These may reflect colonisation by insects during a time when this bed was intermittently dry. Top of shell–free bed is at 455 cm in south face. Scattered quartz coarse sand. The enigma of Bed 6: Green colour; no/rare shells (some in upper 40 cm); homogeneous; thick; very fine sand input; clayey; occasional coarse quartz sand; lack of calcium carbonate; lack of gypsum; occasional concentric mudballs (Fluctuating White Nile, intermittent desiccation).

Bed 7: 455–465 cm main shell bed; abundant *Corbicula* and fish bone in olive sandy clay matrix. Base of shell bed gently undulating and contains scattered 2–3 mm scattered quartz coarse sand /fine gravel. Above shell bed pocket of fibrous gypsum crystals (Littoral/onset of White Nile regression).

Bed 8: 465–600 cm (top of pit) 2.5Y4/1 grey–brown cracking clay. Localised concentration of shells in south face, dominantly *Corbicula*, some *Biomphalaria* and *Melanoides*, mainly about 10 cm above Bed 7 and about 10 cm thick (Swampy flood plain).

A second trench (ES82/2) located 300 m to the east of trench ES82/1 was dug to a depth of 410 cm at the site of borehole ES82/7 which reached a depth of 565 cm. The olive fine sandy clay bed equivalent to Bed 1 in ES82/1 was 125 cm thick at this site and in the lower 80 cm consisted of 30% microcrystalline calcite. Underlying the olive clay was a white clay marl at least 65 cm thick (Fig. 10).

Chronology and implications

Williams *et al.* (2003) have given a full description of the procedures used to date the upper and lower undisturbed cores so that only the ages and their significance are discussed here. Table 3 shows the OSL ages and Table 4 shows the AMS ^{14}C ages. In the upper three beds (6, 7 and 8) both the ^{14}C and the OSL ages become older with increasing depth, as one might expect. This is also the case for the OSL ages obtained for Beds 1 and 2. However, the ^{14}C ages obtained on microcrystalline calcite in Beds 1 and 2 show a scatter of ages between about 36 ka and 44 ka which are far younger than the OSL ages obtained for quartz grains within Beds 1 and 2. This is a clear indication that the microcrystalline calcite precipitated interstitially within Beds 1 and 2 during a time of intense evaporation in the late Pleistocene and that the ages bear no relation to the actual ages of the parent sediments in which they occur. The oxygen isotopic composition of the microcrystalline calcite in a nearby trench (ES3, at 13°35'20"N; 32°40'E) is consistent with this interpretation, as are the calibrated ^{14}C ages of 30,660 ± 800, 41,560 ± 2770 and > 44,360 years BP obtained on microcrystalline calcite at depths of 4.1, 4.6 and 4.8 m, respectively (Williams, 2009, Table 1; Williams *et al.*, 2006, Fig. 8a). When sampling each trench and borehole we examined every microcrystalline calcite and dolomite sample using a field microscope and later confirmed our initial identifications using a Scanning Electron Microscope. We are confident that these sediments are indeed laterally extensive.

The age of Bed 1 remains in doubt. Mean sedimentation rates in Bed 2 amount to 0.15 cm/ka between 430 and 435 cm depth, 1.5 cm/ka between 435 and 450 cm depth, and 0.45 cm/ka between 430 and 450 cm depth. The parent sediments in Bed 1 which is 105 cm thick consist of finely laminated green clays, so that the sedimentation rate would most likely have been lower than in the sands of Bed 2. If we assume a rate of 0.5 cm/ka, the base of Bed 1 would be about 200 ka older than the base of Bed 2 and could date back to about 400 ka. If so, deposition of the green lacustrine clays in Bed 1 may have taken place during Marine Isotope Stage 11 which lasted from 424,000 to 374,000 years ago. Apart from being an unusually long interglacial it was also unusually warm and wet (Raynaud *et al.*, 2005).

Unresolved questions

We noted in the introduction that two key unresolved questions relating to the White Nile are:

a. When did the White Nile first join the main Nile?

b. What type of sediment did the White Nile contribute to the main Nile?

Table 4—Calibrated AMS ^{14}C ages of White Nile sediments collected from trench ES82/1.

Sample no.	Depth (cm)	Bed	Age (years BP)	Material
OZE–300	120	8	14,262 ± 166	S
OZE–583	130	8	14,397 ± 172	S
OZE–301	140	7	14,688 ± 149	S
Wk–10733	486–491	2 (lower)	40,759 ± 518	C
Wk–10732	508–512	1 (upper)	44, 373 ± 519	C
OZE–584	510–513	1 (upper)	38,651 ± 700	C
Wk–10731	525–530	1 (upper)	36,446 ± 313	C

S is shell. C is microcrystalline calcite.

Although the sediments in trench ES82/1 had been dated, the mineralogy of the sediments was not known in any detail. If the basal sediments in the trench have a dominantly volcanic signature, indicating an Ethiopian source, most likely via the Sobat River (Fig. 1a), it would imply that the present–day White Nile issuing from the Lake Plateau of Uganda is a very young river. If the sediments lack volcanic minerals and are primarily quartzose, it would indicate that the White Nile has been flowing in its present valley for at least 240,000 years. Extrapolating sedimentation rates could imply an age of about 400,000 years for the green clay unit (Bed 1) at the base of trench ES82/1. On present admittedly scanty evidence this is about the time that Lake Victoria in Uganda first came into being (Williams & Talbot, 2009). We will now attempt to answer the second question.

METHODS

Light and heavy mineral analysis

Light and heavy mineral analyses were carried out on bulk samples from each bed of trench ES82/1 except for Bed 7, which is a shell breccia. Clays and carbonates were removed by wet sieving and digestion in hydrochloric acid, and grains in the size range 125 to 180 µm were selected for the analyses by dry sieving. This particle size range coincides best with the grain size modes for all the samples. Heavy and light minerals were separated using heavy liquid tetrabromoethane and the grains were mounted in epoxy (heavy minerals) or lakeside balsam (light minerals), thin sectioned and point counted. A total of 700 grains was counted for each slide in the case of the light minerals, and a total of 300 grains for the heavy minerals except for Bed 8 where only 200 grains were counted on account of the small sample size. The results of the analyses are shown in Tables 5a and b.

Roundness analysis

The roundness analysis was conducted by comparing grain shapes with the grain roundness images catalogued by Powers (1953). To avoid any possible bias, the labels of the light mineral slides were covered when conducting the picture match. 500 grains were counted for each slide. Table 6 shows the results of the roundness analysis.

Clay mineral analysis

An X–ray diffraction survey of the long and short cores collected from the side of trench ES82/1 was done at the South Australian Museum with an Aeris X–ray powder diffractometer and processed with the associated Highscore Plus program (version 4.9). The mineral composition was assessed with the Rietveld system to give the mineral percentages presented in Table 7. Montmorillonite clay (smectite) does not have a well–defined structure and so could not be readily used for Rietveld analysis. A Muscovite 2–M pattern was used to model the montmorillonite in the Rietveld analysis. In this survey only mg samples were used so selected 6 to 10 g samples were sent to the CSIRO laboratory at Urrbrae in South Australia to confirm the clay analysis. At the CSIRO laboratory the bulk samples were micronized using a McCrone micronizing mill with ethanol and the unknown mix of interlayer cations (both monovalent and divalent) were exchanged with calcium. Micronizing removes particle size effects, which are common with coarse quartz and feldspar minerals. Calcium exchange sharpens the (001) clay peaks making phase identification and quantification more definitive.

In order to confirm the identity of the clay minerals, the clay fraction (nominally < 2 µm) was separated from the bulk materials using the following procedure. Approximately 3–10 g of the as received samples were dispersed by vigorously shaking with 1M NaCl solutions. From this dispersion the < 2 µm and > 2 µm size fractions were collected by repeated washing with de–ionized water, ultra–sonification and centrifugation. At the completion of each step, the supernatants from the centrifugation were collected in 1 litre beakers. The collected < 2 µm fractions were recovered by flocculation using excess NaCl and centrifugation. The recovered materials were twice washed with acetic acid solution (approximately 0.2 M) to remove carbonates, twice

washed with $CaCl_2$ solution (approximately 0.2 M), once washed with high–purity water, and once washed with ethanol. High speed centrifugation was used to collect the samples after each wash. After the ethanol wash the samples were dried in an oven set to 60°C then thoroughly mixed in an agate mortar and pestle before being lightly backpressed into stainless steel sample holders for XRD analysis.

XRD patterns were recorded with a PANalytical X'Pert Pro Multi–purpose Diffractometer using Fe filtered Co Kα radiation, automatic divergence slit, 2° anti–scatter slit and fast X'Celerator Si strip detector. Quantitative analysis was done with program TOPAS (V6) by Bruker, which is a Rietveld–based X–ray profile fitting software for structure and quantitative phase analysis. This analysis incorporated calibrations for the highly disordered smectite phase. The results are given in Table 8 and Fig. 12. Analysis of the XRD data confirms that there is no mica (i.e., muscovite) present and corroborates our initial survey results.

Table 5—(a) Percentage composition of light mineral assemblages in Section ES82/1. (b) Percentage composition of heavy mineral assemblages in Section ES82/1

Bed	**1**	**2**	**3**	**4**	**5**	**6b**	**6m**	**8**
Unstrained quartz	61.1	63.2	57.2	54.4	55.2	53.3	51.1	45.7
Strained quartz	31.8	29.4	34.7	39.4	39.0	41.0	42.2	48.5
Vein quartz	0.7	1.7	1.3	1.0	0.3	0.1	0.5	1.2
Polycrystalline quartz	0.3	0.3		0.1	0.4			
Ribbon quartz	0.4	0.4						
TOTAL QUARTZ	94.3	95.0	93.2	94.9	94.9	94.4	93.8	95.4
K–feldspar	5.4	4.4	6.5	4.2	4.4	5.5	5.7	4.2
Plagioclase		0.2	0.1	0.7	0.5		0.2	0.1
TOTAL FELDSPAR	5.4	4.6	6.6	4.9	4.9	5.5	5.9	4.3
Rock fragments	0.1	0.1	0.0	0.0	0.0	0.0	0.0	0.0
TOTAL	**99.8**	**99.7**	**99.8**	**99.8**	**99.8**	**99.9**	**99.7**	**99.7**

(a)

Bed	**1**	**2**	**3**	**4**	**5**	**6b**	**6m**	**8**
Metamorphic								
Epidote	37.3	39.6	17.6	16.0	22.6	21.0	28.3	21.0
Hornblende	10.3	9.0	9.0	7.9	9.3	7.7	8.6	1.8
Garnet	2.3	1.3	4.0	7.6	6.2	6.9	6.6	9.0
Kyanite	1.3	1.6	2.0	2.3	2.0	1.3	1.3	1.5
Staurolite	1.6	1.0	1.6	4.0	7.0	4.0	5.6	4.2
Recycled sedimentary								
Tourmaline	9.9	7.0	8.6	4.3	5.3	11.3	5.3	11.6
Zircon	3.3	3.3	1.3	3.6	2.3	3.0	0.6	0.0
Rutile	3.3	0.6	3.0	0.6	0.6	1.3	0.6	2.0
Opaques	30.3	36.3	52.6	53.3	44.3	43.3	42.6	49.0
TOTAL	**99.6**	**99.7**	**99.7**	**99.6**	**99.6**	**99.8**	**99.5**	**100.1**

(b)

6b: base of Bed 6. 6m: middle of Bed 6. Analyses were not carried out on Bed 7, which was composed largely of shell fragments. Opaque minerals were not individually identified. Percentages were obtained by point counting as described in the text.

RESULTS AND INTERPRETATION

Light and heavy mineral analysis

The light minerals (Table 5a) show insignificant change over the eight stratigraphic levels sampled. Quartz accounts for about 95% of the light mineral content throughout the section, and the remaining fraction consists almost entirely of potassium feldspar, with only traces of plagioclase. This is highly indicative of a silicic plutonic or metamorphic source. The presence of a substantial component of strained quartz and traces of polycrystalline quartz indicates that at least some of the material is of metamorphic provenance. The low percentage of feldspar may be due to prolonged abrasion and weathering, or to a lack of feldspar in the source area. The first possibility seems more likely, since the probable source areas such as the Nuba Mountains and the basement rocks of the White Nile headwaters are feldspar rich (Vail, 1974, 1976, 1978; Garzanti *et al.*, 2015; Williams, 2019, Fig, 4.3).

Apart from opaque minerals, which were not individually identified, the dominant heavy minerals (Table 5b) are epidote, green hornblende, garnet, kyanite and staurolite. All of these minerals point to a high–grade metamorphic source. A few euhedral zircon crystals are present, which taken alone could signify either a volcanic or a plutonic igneous source. However, most zircons, rutiles and tourmalines are rounded, suggesting a recycled sedimentary source as indicated in Table 5b. The absence of any material that would indicate a volcanic source is also supportive of plutonic or metamorphic provenance, although this is not in itself diagnostic since volcanic minerals such as pyroxene, olivine and volcanic glass are much less stable and less likely to be preserved than the minerals mentioned above.

In summary, the content of light and heavy minerals is consistent with the material in all the beds except Bed 3 having been derived ultimately from metamorphic and plutonic igneous sources such as the Nuba Mountains to the west and the basement rocks of the Ugandan White Nile headwaters. Bed 3 differs from all the other beds in being locally derived. It is very poorly sorted and has a high percentage of feldspar. It was most likely deposited during a flash flood emanating from the granitic rocks that crop out in the two low hills of Jebel Tomat located 11 km east of trench ES82/1. Part of the Jebel Tomat outcrop consists of augen gneiss which Vail (1982, p. 52) describes as ‘a porphyroblastic quartzo–feldspathic gneiss’ which was probably formed by recrystallization of the basement rocks.

Roundness analysis

The roundness analysis (Table 6) shows that the grains investigated in Beds 1 and 3 were dominantly angular and indicative of high energy flow. The other beds contain a relatively high proportion of rounded grains consistent with an influx of wind–blown sand during locally drier intervals. The high proportion of very fine sand particles in the size range 125–150 in the lower core (Fig. 11; Table 2b) offers support for this inference.

Clay mineral analysis

The core pilot study results given in Table 7 show that the lower and longer core (Lx) has clay (modelled as muscovite mica), quartz and dolomite. The mineral amounts vary widely through time. The upper and shorter core (Sx) is also highly variable but has calcite rather than dolomite. The key finding is confirmed in Table 8 which shows that the principal minerals other than quartz are smectite, illite and interstratified illite–smectite. Table 8 has the pilot study results and in brackets the selected sample results. The sum of the mineral values is compared to the muscovite modelled values of the pilot study. The agreement with the data shown in Table 7 is quite good especially as the pilot study used mg samples and the selected samples ranged from 6 g to 10 g. This latter amount would represent a longer time interval and so is not strictly comparable to the smaller samples.

Fig. 12 shows the high d–spacing profiles for the calcium–exchanged selected samples. The clays are identified as dioctahedral smectite, however, the position of the 060 peak suggests either montmorillonite or beidellite but less likely nontronite. We have chosen to call the clay montmorillonite in the Fig. but recognise it by the broader term smectite.

Table 6—Point–count percentages of the light minerals in Section ES82/1, using Powers’ (1953) grain roundness images.

Bed	**1**	**2**	**3**	**4**	**5**	**6b**	**6m**	**8**
Very angular	8.4	3.0	2.4	1.6	2.4	2.8	1.8	1.0
Angular	33.8	23.0	31.4	24.8	23.8	23.6	18.6	22.6
Sub–angular	29.4	39.0	28.2	29.2	33.4	33.4	32.6	38.2
Sub–rounded	19.6	26.8	24.8	26.4	30.4	27.4	31.8	26.0
Rounded	8.4	7.8	12.4	17.2	9.4	10.8	11.8	11.2
Well rounded	0.4	0.4	0.8	0.8	0.6	2.0	0.4	1.0

Table 7—X–ray diffraction pilot study (mineral %) of the ES82/1 monoliths at 1 cm intervals.

Short core ES82 1.7 to 1.2 m

ID numbers in centimetres from base 1.7 m end

	Clays modelled as			Low peak
ID	**Musco-vite**	**Quartz**	**Calcite**	**d–spacing**
S1	39	44	17	10
S5	49	29	22	10
S9	48	29	23	10
S13	34	19	47	10.4
S16	51	33	16	10, broad
S20	52(39)	38(45)	10(10)	10, broad
S23	46	39	15	10, broad
S27	15	72	13	broad
S31	15	27	58	broad
S33	2	87	12	none
S35	24	9	67	none
S37	50	38	12	13.7
S39	2	98	0	none
S42	22	9	69	13.5
S44	15	82	3	broad
S48	58(57)	28(24)	14(7)	13.5
S50	53	40	7	12.9

Long core ES82 5.3 m to 4.3 m

ID number in centimetres from the 5.3 end

	Clays modelled as			Low peak
ID	**Musco-vite**	**Quartz**	**Dolomite**	**d–spacing**
L1	53(42)	18(22)	29(31)	12.5
L6	88	1	11	12.5
L12	25	74	2	12.5
L24	0	14	86	none
L39	2	97	1	12.5
L42	2.3	19	78	12.5
L48	0	13	86	none
L53	27	58	15	12.9
L72	1.2	49	50	none
L87	2	98	0	none
L94	0.6	86	14	none

Numbers in brackets are the sum of the smectite and Illite/Illite–smectite values from Table 7

Fig. 12 indicates the significance of montmorillonite in samples L1 and S48. Sample S20 has relatively weak peaks at high d–spacing for both montmorillonite and illite, indicating likely randomly interstratified clay species containing smectite layers. The montmorillonite (Ca) reference pattern has its high d–spacing peak (001) at 15Å as shown in Fig. 12. This spacing contracts when the interlayer cation is composed of a variety of hydrated monovalent and divalent cations. In the Lower (L) core, the high d–spacing peaks listed in Table 8 between 12.5 and 12.9 could be assigned as smectite or interstratified illite–smectite. Higher up the core, samples L48 and L72 to L94 have no prominent peaks and hence there is little evidence of smectite in these samples and no evidence of illite and illite/smectite in these sections of the Lower core.

The short (S) core data are more complex. The S20 scan shows that the 10 Å peak relates to illite, and the higher d–spacing to smectite. The lower portion of the core data consists of mixed smectite and illite. Sample S35 and above show a return to smectite, with peaks between 12.9 Å and 13.7 Å.

DISCUSSION

The work of Ducassou *et al.* (2008, 2009), Revel *et al.* (2010, 2015), Blanchet *et al.* (2013, 2015) and Hennekam *et al.* (2014) has confirmed that clastic muds rich in continental organic matter and highly organic sapropels accumulated on the floor of the eastern Mediterranean during phases of very high Nile flow. Comparison with dated alluvial sediments in the lower Blue and White Nile valleys (Williams *et al.*, 2015) has shown that times of high flow in the Blue and White Nile coincide very broadly with sapropel units S8 (217 ka), S7 (195 ka), S6 (172 ka), S5 (124 ka), S3 (81 ka), S2 (50 ka) and S1 (ca. 13–5 ka).

Bastian *et al.* (2017) analysed the clay minerals in a sediment core recovered from the Nile deep sea fan spanning the last 32 ka and compared their results with independently dated evidence from Lake Tana in Ethiopia, from which flows the Blue Nile. They found that there was an abrupt response of chemical weathering of silicate rocks to changes in the strength of the summer monsoon. The changes in the proportion of smectite clay minerals in our White Nile sediment samples are also a probable result of alternating wet and dry climatic phases in the White Nile catchment during at least the last 240 ka and possibly the last 400 ka.

Mineral composition of White Nile sediments

Previous workers have investigated the composition of sediments transported by the Nile and its major tributaries but have focussed mainly upon sediments transported by these rivers at the present time. In a classic study of the mineralogy of Nile sediments, Shukri (1950) carried out a detailed analysis of sediments collected from the headwaters of the White Nile, the Blue Nile, and the Atbara downstream as far

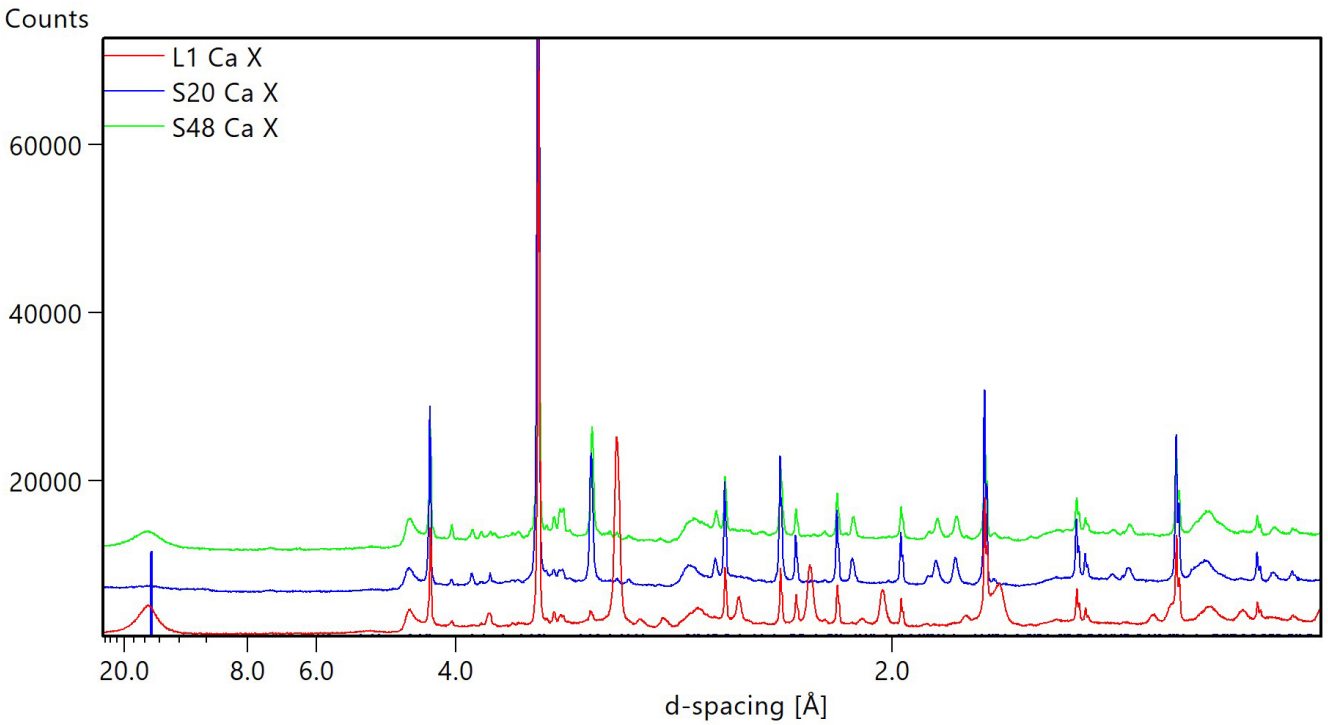

Fig. 12—X–ray diffraction analysis of treated selected clay samples from trench ES82/1.

as the Nile Delta. He found that sediments in the White Nile and its tributaries contained abundant minerals diagnostic of a metamorphic provenance and a virtual absence of minerals like augite that indicate a volcanic provenance. The Blue Nile and the Atbara were almost entirely dominated by volcanic minerals. Recent very detailed work by Garzanti *et al.* (2006, 2015) has confirmed Shukri's pioneering findings while adding significant detail. Once again, the analyses have been confined to modern Nile sediments. There is strong consensus among all investigators about the nature and provenance of light and heavy minerals in the White Nile on the one hand and the Blue Nile and Atbara on the other. However, when it comes to the clay minerals present in the sediments there is less agreement, for reasons we explain.

The magisterial study by Garzanti *et al.* (2015) is by far the most comprehensive study of clay minerals in the Nile Basin. In the well–drained wet highlands of the East African Rift, the dominant clay mineral is kaolinite, with lesser amounts of gibbsite and illite. The alluvial and lacustrine sediments of central Uganda, which are derived from 'Precambrian granitoid gneisses and metasediments, are dominated by kaolinite and quartz, with minor smectite, chlorite, and illite/muscovite' (op. cit., 2015, p. 29). However, the situation is quite different in South Sudan, where 'the

Table 8—X–ray diffraction results (mineral %) of treated selected samples.

ID	Quartz	Smectite	Illite/ Illite–Smectite	Dolomite	Calcite	Albite/ Anorthite	Microcline	Kaolin
Bulk								
L1	22	42		31	< 1	2	2	< 1
S20	45	13	26	< 1	10	3	2	1
S48	24	40	17	< 1	7	6	3	2
< 2 µm fraction								
L1	< 1	98						1
S20	1	24	67			2		4
S48	1	63	27			1	< 1	7

alkaline soils of the alluvial to swampy lowlands are smectite–rich with subordinate kaolinite, chlorite and illite' (op. cit., 2015, p. 29). Conditions change once more on reaching the northern Gezira region in central Sudan (Fig. 2), where the sediments along the Blue and White Nile differ very little and consist of smectite with subordinate amounts of kaolinite, vermiculite, illite and chlorite (op. cit., 2015, pp. 29–30). The reason for this lack of difference is very simple: the Gezira alluvial fan was built up by the Blue Nile and its distributary channels and the youngest and most northerly of these former Blue Nile channels have remained active until the early Holocene (Williams, 2019, pp. 153–4).

To find out what sort of material Mesolithic and Neolithic potters used to temper their wares, Lara Maritan and her co–workers collected bulk samples of clay from the banks of the White Nile, the Blue Nile, the main Nile, and the Atbara rivers (Maritan *et al.*, 2021). They used a combination of petrographic analysis under polarized light, X–ray powder diffraction (XRPD), bulk geochemical analysis by X–ray fluorescence (XRF) and strontium isotope analysis to determine the composition of their bulk samples. The results obtained by Maritan *et al.* (2021) were entirely consistent with the results obtained by Garzanti *et al.* (2015), with both groups of investigators noting the admixture of Blue and White Nile sediments in the northern Gezira.

The distal reaches of the oldest and least well–defined Blue Nile palaeochannel lie somewhat north of latitude 14°N (Fig. 8). Esh Shawal lies well south of any possible influence from former Blue Nile channels and is sheltered by the Managil Ridge (Figs 1c, 8). Our clay mineral and petrographic data are therefore more likely to reflect the unadulterated type of sediments brought to the White Nile from its Ugandan headwaters than data obtained from the White Nile north of about 14°N.

Depositional environments in the White Nile Valley

The new data we have presented here relating to the stratigraphy and composition of Quaternary alluvial sediments in the lower White Nile Valley allow us to suggest the following sequence of events.

(a) During a prolonged arid interval with a probable age > 400 ka, there was widespread precipitation of microcrystalline high magnesian calcite and dolomite and accumulation of white calcareous marls in broad shallow depressions east of the lower White Nile between 13°30′N and 14°15′ N (Fig. 2). (This unit was absent from trench ES82/1 but was present in trench ES82/2 located 300 m further east: see Fig. 10).

(b) This arid interval was succeeded by a very long wet phase, possibly coeval with Marine Isotope Stage 11 (424–374 ka) and possibly coinciding with the inception of Lake Victoria in the Lake Plateau of Uganda. Finely laminated green lacustrine clays were laid down in a former White Nile Lake which attained a maximum elevation of about 386 m, or 8 m above the unregulated mean maximum White Nile flood level in this locality. The heavy mineral assemblage indicates a silicic plutonic or metamorphic source and is consistent with derivation from the Archaean Gneiss–Granulite Complex that underlies the Lake Plateau in Uganda. The dominance of smectite among the clay minerals is consistent with poorly drained or swampy conditions as the lake receded. The quartz grains within the clay sediments were angular, which is consistent with initially high energy flow from the rugged escarpment of the Ugandan Lake Plateau via the appropriately named Bahr el Jebel ('River of the Mountain') down to the swampy plains of South Sudan (Fig. 1a).

(c) There was a return to drier conditions following deposition of the finely laminated green clay accompanied by high energy flow and deposition of olive yellow clayey fine sands. Initial deposition of the sands was accompanied by erosional scouring of the underlying green clays. The relatively high proportion of rounded quartz grains is consistent with an influx of wind–blown sand during locally drier intervals. Deposition of the sandy alluvium extended from well before 210 ka to well after 166 ka, but the precise age of this unit remains elusive. The heavy minerals are once again consistent with a source on the Ugandan Lake Plateau. Smectite is sporadically present in this unit, suggesting that on occasion conditions were not conducive to smectite formation, possibly during brief arid phases associated with carbonate precipitation. The sands occur up to an elevation of about 381 m, or 3 m above the historic mean maximum unregulated White Nile flood level.

(d) The next event has both local and regional implications. A narrow band of sub–angular quartz gravel was laid down by a sheet flood flowing from Jebel Tomat during an intense downpour. Sheet floods are characteristic of gently sloping desert regions devoid of vegetation. The gravel band extends down to an elevation of 376 m near Esh Shawal, or 2 m lower than the historic unregulated White Nile flood level at this site. The White Nile was therefore at a very low level with much reduced summer discharge, and the regional climate was probably similar to that in the desert regions of northern Sudan today. The age of this event is not known but was younger than 166 ka.

(e) There was a brief return to wetter conditions during which a thin layer of green very fine sandy clay was deposited over the sheet flood gravels. This unit is slightly calcareous, suggesting that the climate during deposition was seasonally arid, as it is today. The rounded nature of many of the fine sandy quartz grains suggests some input from desert dust.

(f) Deposition of the thin green sandy clay was followed by deposition of a thin layer of olive yellow calcareous clayey fine sand, as in (c). The microcrystalline calcite points to seasonal or post–depositional desiccation. The rounded nature of the quartz grains is again indicative of a desert dust input, possibly during dust storms blowing from the northern desert along the Nile Valley before the onset of the rainy season, as is common in this region today (Griffiths & Soliman, 1972).

(g) Deposition of the olive–green fine clayey sand was succeeded by the accumulation of several metres of olive brown sandy clay with frequent insect galleries in the lower 150 cm and sporadic mudballs and occasional pockets of coarse sand. The presence of fine vertical and oblique cracks is evidence of seasonal desiccation, as is the presence of insect galleries and the presence of 10–20% carbonate. Precipitation of microcrystalline high magnesian calcite was already under way by 45 ka and continued intermittently until at least 30 ka. It was caused by evaporative concentration of groundwater during a period of progressive climatic desiccation. The absence of any horizontal bedding is probably due to disturbance from insects and homogenisation of the parent sediment. Deposition probably took place during a time of fluctuating White Nile flood levels and intermittent desiccation. Maximum desiccation was during the Last Glacial Maximum (21 ± 3 ka) when Lake Victoria and Lake Albert dried out (Livingstone, 1980; Johnson *et al.*, 1996; Stager & Johnson, 2008) and flow in the White Nile was reduced to a trickle. Lake Tana, the source of the Blue Nile in Ethiopia (Fig. 1b), also dried out at this time (Lamb *et al.*, 2007; Marshall *et al.*, 2011). Soils formed on the dry floor of Lake Albert have AMS ^{14}C ages of 20.75–17.75 ka and 16.73–15.1 ka indicating that these were times of no flow to the White Nile from the lakes of Uganda (Williams *et al.*, 2006: Fig. 9b). The upper 15 cm of this unit appear to have been laid down during the very late Pleistocene and have OSL ages of 21.0 ± 2.6 ka and 16.3 ± 2.2 ka suggesting that there was probably some local input–or remobilisation–of sediment from tributaries like the Bahr el Jebel in South Sudan (Fig. 1). The heavy minerals in this and the proceeding two depositional units (e) and (f) indicate a silicic plutonic or metamorphic source consistent with sediment transport from the Lake Plateau of Uganda. The principal clay minerals in the upper portion of this unit are smectite, illite and interstratified illite–smectite.

(h) The abrupt return of the summer monsoon about 15,000–14,500 years ago saw major flooding in the White Nile Valley and the creation of a seasonal lake which reached a maximum elevation of 382 m by about 14.5 ka, at which time it began to recede. Pockets of coarse quartz sand and fine gravel appear to indicate the presence of a former lake shoreline or beach. The retreat of this lake is recorded in a shell breccia about 10 cm thick with three calibrated AMS ^{14}C ages for sub–fossil aquatic snail shells of 14.3 ka, 14.4 ka and 14.7 ka. The presence of fibrous gypsum crystals above the shell bed indicates desiccation after the lake regression.

(i) From about 12 ka onwards both the Desert Nile and the Blue Nile began to erode vertically downwards, causing the White Nile to follow suit. A detailed analysis of the likely causes of this incision is given in Williams (2019, pp.153–4). During times when the Blue Nile was operating as a bed load river, aggradation was dominant. Conversely, once the Blue Nile became a suspension load river, during warmer, wetter climatic intervals in its Ethiopian headwaters, it began to incise, as did the main Nile. As the White Nile incised, previously swampy portions of its flood plain dried out. Seasonal flooding along the White Nile continued throughout the Holocene with the progressive deposition of about 1.5 m of grey–brown cracking clay. The dominant clay mineral in this sediment is smectite. At intervals throughout the Holocene there were short–lived periods of high flood level during which aquatic snail shells were laid down and subsequently buried beneath alluvial clay. ^{14}C ages obtained for the shells indicate higher than present White Nile flood levels at 9.7–9.0 ka, 7.9–7.6 ka, 6.3 ka and 3.2–2.8 ka (Williams, 2009).

CONCLUSION

There is no dispute that the dominant clay mineral in the volcanic sediments transported by the Blue Nile and Atbara rivers via the Desert Nile to the Nile deep sea fan in the eastern Mediterranean is smectite. For at least 30 million years smectite clays of Ethiopian provenance have been accumulating in the Nile deep sea fan. However, the presence of smectite in the fan sediments does not mean that they were solely derived from Ethiopia. Our work has shown for the first time that the White Nile has been transporting smectite–rich sediments from the time of its probable inception over 240 ka ago and possibly since about 400 ka. Our analysis of the heavy mineral assemblages in White Nile alluvial sediments provides strong support for a source in the Lake Plateau region of Uganda. The White Nile was flowing from Uganda by at least 240 ka and very likely from about 400 ka. Flow in the White Nile has fluctuated in response to regional fluctuations in climate. During times when the summer monsoon was stronger than today there was widespread flooding in the White Nile Valley. The two most recent periods of widespread flooding were the Last Interglacial at about 125 ka and the terminal Pleistocene at about 15–14.5 ka. Both events are also evident in the Nile deep sea fan, with the accumulation of highly organic sapropel beds at these times. The White Nile alluvial record has significant gaps but does provide a much more complete alluvial record than the Blue Nile which has a

much steeper flood gradient and a more erosive flood regime. It is probable that periodic lateral migration of the White Nile across its former flood plains has removed a significant but unknown portion of its Quaternary alluvial record. Losses caused by vertical incision seem relatively minor.

Acknowledgements—*This paper is dedicated to the memory of Don Adamson, who worked with MAJW in the Nile Valley between 1973 and 1983 and whose powers of observation were only equalled by his enthusiasm for the Nile. We thank Adrian Beech, CSIRO Land & Water, for the grain size analyses.*

REFERENCES

Adamson DA, Gillespie R & Williams MAJ 1982. Palaeogeography of the Gezira and of the lower Blue and White Nile valleys. *In:* Williams MAJ & Adamson DA (Editors)–A Land between Two Niles: Quaternary geology and biology of the Central Sudan. Balkema, Rotterdam, pp. 165–219.

Adamson D & Williams F 1980. Structural geology, tectonics and the control of drainage in the Nile Basin. *In:* Williams MAJ & Faure H (Editors)–The Sahara and The Nile: Quaternary Environments and Prehistoric Occupation in Northern Africa. Rotterdam, A.A. Balkema, pp. 225–252.

Adamson D, McEvedy R & Williams MAJ 1993. Tectonic inheritance in the Nile Basin and adjacent areas. Israel Journal of Earth Sciences 41: 75–85.

Avni Y, Segev A & Ginat H 2012. Oligocene regional denudation of the northern Afar dome: Pre–and syn–breakup stages in the Afro–Arabian Plate. Geological Society of America Bulletin 124: 1871–1897.

Barrows TT, Williams MAJ, Mills SC, Duller GAT, Fifield LK, Haberlah D, Tims SG & Williams FM 2014. A White Nile megalake during the last interglacial period. Geology 42: 163–166.

Bastian L, Revel M, Bayon G, Dufour A & Vigier N 2017. Abrupt response of chemical weathering to Late Quaternary hydroclimate changes in northeast Africa. Scientific Reports 7: 44231. https://doi.org/10.1038/srep44231.

Blanchet CL, Tjallingii R, Frank M, Lorenzen J, Reitz A, Brown K, Feseker T & Brückmann W 2013. High–and low–latitude forcing of the Nile River regime during the Holocene inferred from laminated sediments of the Nile deep–sea fan. Earth and Planetary Science Letters 364: 98–110.

Blanchet CL, Contoux C & Leduc G 2015. Runoff and precipitation dynamics in the Blue and White Nile catchments during the mid–Holocene: A data–model comparison. Quaternary Science Reviews 130: 222–230.

Bowen R & Jux U 1987. Afro Arabian geology. A kinematic view. London, Chapman & Hall.

Corti G 2009. Continental rift evolution: From rift initiation to incipient break–up in the Main Ethiopian Rift, East Africa. Earth–Science Reviews 96: 1–53.

Ducassou E, Mulder T, Migeon S, Gonthier E, Murat A, Revel M, Capotondi L, Bernasconi SM, Mascle J & Zaragosi S 2008. Nile floods recorded in deep Mediterranean sediments. Quaternary Research 70: 382–391.

Ducassou E, Migeon S, Mulder T, Murat A, Capotondi L, Bernasconi M & Mascle J 2009. Evolution of the Nile deep–sea turbidite system during the Late Quaternary: influence of climate change on fan sedimentation. Sedimentology 56: 2061–2090.

El Badri O 1972. Sediment transport and deposition in the Blue Nile at Khartoum, flood seasons 1967, 1968 and 1969. MSc thesis, University of Khartoum.

Fielding L, Najman Y, Millar I, Butterworth P, Ando S, Padoan M, Barfod D & Kneller B 2016. A detrital record of the Nile River and its catchment. Journal of the Geological Society doi: 10.1144/jgs2016–075.

Fielding L, Najman Y, Butterworth P, Garzanti E, Vezzoli G, Barfod D & Kneller B 2018. The initiation and evolution of the river Nile. Earth and Planetary Science Letters 489: 166–178.

Fritz H, Abdelsalam M, Ali KA, Bingen B, Collins AS, Fowler AR, Ghebreab W, Hauzenberger CA, Johnson PR, Kusky TM, Macey P, Muhongo S, Stern RJ & Viola G 2013. Orogen styles in the East African Orogen: A review of the Neoproterozoic to Cambrian tectonic evolution. Journal of African Earth Sciences 86: 65–106.

Garzanti E, Andò S, Vezzoli G, Megid AA & Kammar A 2006. Petrology of Nile River sands (Ethiopia and Sudan): sediment budgets and erosion patterns. Earth and Planetary Science Letters 252: 327–341.

Garzanti E, Andò S, Padoan M, Vezzoli G & El Kammar A 2015. The modern Nile sediment system: processes and products. Quaternary Science Reviews 130: 9–56.

Griffiths JF & Soliman KH 1972. The Northern Desert (Sahara). *In*: Griffiths JF (Editor)–Climates of Africa. World Survey of Climatology, Volume 10. Amsterdam, Elsevier, pp. 75–131.

Gunn RH 1982. The plains of the central and southern Sudan. *In:* Williams MAJ & Adamson DA (Editors)–A Land between Two Niles: Quaternary geology and biology of the central Sudan, A.A. Balkema, Rotterdam, pp. 81–109.

Hennekam R, Jilbert T, Schnetger B & de Lange GJ 2014. Solar forcing of Nile discharge and sapropel S1 formation in the early–to mid–Holocene. Paleoceanography 29: 2013PA002553.

Hofmann C, Courtillot V, Férard G, Rochette P, Yirgus G, Ketefo E & Pik R 1997. Timing of the Ethiopian flood basalt event and implications for plume birth and global change. Nature 389: 838–841.

Hunting Technical Services Limited 1964. The White Nile East Bank, Rabak to Khartoum: Soils and Engineering Reconnaissance. Roseires Soil Survey Report No. 6, 1–128. Khartoum, Republic of the Sudan, Ministry of Agriculture.

Hunting Technical Services Limited 1965. Report No 11. The White Nile East Bank Melut to Rabak, exploratory soils and engineering survey. Khartoum, Republic of the Sudan, Ministry of Agriculture.

Hurst HE 1952. The Nile: a general account of the river and the utilisation of its waters, 2nd Edition. London, Constable, 326 pp.

Johnson TC, Scholz CA., Talbot MR, Kelts K, Ricketts RD, Ngobi G, Beuning K, Ssemmanda I & McGill JW 1996. Late Pleistocene desiccation of Lake Victoria and rapid evolution of cichlid fishes. Science 273: 1091–1093.

Lamb HF, Bates CR, Coombes PV, Marshall MH, Umer M, Davies SJ & Dejen E 2007. Late Pleistocene desiccation of Lake Tana, source of the Blue Nile. Quaternary Science Reviews 26 (3–4): 287–299.

Livingstone DA 1980. Environmental changes in the Nile headwaters. *In:* MAJ Williams & H Faure (Editors)–The Sahara and the Nile. Quaternary Environments and Prehistoric Occupation in Northern Africa, Rotterdam, AA Balkema, pp. 339–359.

Lombardini E 1864. Saggio idrologico sul Nilo. Milan, Italy.

Lombardini E 1865. Essai sur l'hydrologie du Nil. Paris, France.

Leplongeon A, Goder–Goldberger M & Pleurdeau D (Editors) 2020. Human occupations of the Nile Valley and neighbouring regions between 75,000 and 15,000 years ago. National Museum of Natural History, Paris.

Maritan L, Gravagna E, Cavazzini G, Zerboni A, Mazzoli C, Grifa C, Mercurio M, Mohamed AA, Usai D & Salvatori S 2021. Nile River clayey materials in Sudan: chemical and isotope analysis as reference data for ancient pottery provenance studies, Quaternary International 2021, doi: https://doi.org/10.1016/j.quaint.2021.05.009.

Marshall MH, Lamb HF, Huws D, Davies SJ, Bates R, Bloemendal J, Boyle J, Leng MJ, Umer M & Bryant C 2011. Late Pleistocene and Holocene drought events at Lake Tana, the source of the Blue Nile. Global and Planetary Change 78: 147–161.

Mather CC 2020. Dolomite formation within groundwater systems of arid northwest Australia. Unpublished PhD thesis, University of Western Australia.

McDougall I, Morton WH & Williams MAJ 1975. Age and rates of denudation of Trap Series basalts at Blue Nile gorge, Ethiopia. Nature 254: 207–209.

Padoan M, Garzanti E, Harlavan Y & Villa IM 2011. Tracing Nile sediment sources by Sr and Nd isotope signatures (Uganda, Ethiopia, Sudan). Geochimica et Cosmochimica Acta 75: 3627–3644.

Powers MC 1953. A new roundness scale for sedimentary particles. Journal of Sedimentary Research 23 (2): 117–119.

Raynaud D, Barnola JM, Souchez R, Lorrain R, Petit JR, Duval P & Lipenkov VY 2005. Palaeoclimatology: the record for marine isotope stage 11. Nature 436: 39–40.

Revel M, Ducassou E, Grousset FE, Bernasconi SM, Migeon S, Revillon S, Mascle J, Murat A, Zaragosi S & Bosch D 2010. 100,000 years of African monsoon variability recorded in sediments of the Nile margin. Quaternary Science Reviews 29: 1342–1362.

Revel M, Ducassou E, Skonieczny C, Colin C, Bastian L, Bosch D, Migeon S & Mascle J 2015. 20, 000 years of Nile River dynamics and environmental changes in the Nile catchment area as inferred from Nile upper continental slope sediments. Quaternary Science Reviews 130: 200–221.

Shukri NM 1950. The mineralogy of some Nile sediments. Quarterly Journal of the Geological Society 105: 511–534.

Sir Alexander Gibb & Partners 1954. Estimation of irrigable areas in the Sudan 1951–3. Report to the Sudan Government. Metcalf and Cooper Ltd., London.

Stager JC & Johnson TC 2008. The Late Pleistocene desiccation of Lake Victoria and the origin of its endemic biota. Hydrobiologia 596: 5–16.

Talbot MR & Williams MAJ 2009. Cenozoic evolution of the Nile Basin. *In:* Dumont HJ (Editor)–The Nile: Origin, environments, limnology and human use, Monographiae Biologicae 89, Dordrecht, The Netherlands, Springer, pp. 37–60.

Talbot MR, Williams MAJ & Adamson DA 2000. Strontium isotope evidence for late Pleistocene reestablishment of an integrated Nile drainage network. Geology 28: 343–346.

Tothill JD 1946. The origin of the Sudan Gezira clay plain. Sudan Notes and Records 27: 153–183.

Tothill JD 1948. A note on the origins of the soils of the Sudan from the point of view of the man in the field. *In:* Tothill JD (Editor)–Agriculture in the Sudan. Oxford, Oxford University Press, pp. 129–143.

USDA 1996. United States Department of Agriculture, Natural Resources Conservation Service, National Soil Survey Center, Soil Survey Laboratory Methods Manual. Soil Survey Investigations Report No. 42.

Vail JR 1974. Geological map of the Democratic Republic of Sudan and adjacent areas, at scale 1: 2 000 000. Ministry of Overseas Development (British Government) Publication DOS 1203B.

Vail JR 1976. Outline of the geochronology and tectonic units of the Basement complex of north–east Africa. Proceedings of the Royal Society of London 350A: 127–141.

Vail JR 1978. Outline of the geology and mineral deposits of the Democratic Republic of the Sudan and adjacent areas. Overseas Geology and Mineral Resources No 49, 68 pp. London, Her Majesty's Stationary Office.

Vail JR 1982. Geology of the central Sudan. *In*: Williams MAJ & Adamson DA (Editors)–A Land between Two Niles: Quaternary geology and biology of the central Sudan. Balkema, Rotterdam, pp. 51–63.

Vermeersch P 2020. Human occupation density and mobility in the lower Nile Valley (75,000–15,000 years ago). *In:* Leplongeon A, Goder–Goldberger M & Pleurdeau D (Editors)–Not Just a Corridor: Human occupations of the Nile Valley and neighbouring regions between 75,000 and 15,000 years ago. National Museum of Natural History, Paris, pp. 139–157.

Vermeersch PM & Van Neer W 2015. Nile behaviour and Late Palaeolithic humans in Upper Egypt during the Late Pleistocene. Quaternary Science Reviews 130: 155–167.

Willcocks W 1904. The Nile in 1904. London, E. & F.N. Spon, 225 pp.

Williams FM, Williams MAJ & Aumento F 2004. Tensional fissures and crustal extension rates in the northern part of the Main Ethiopian Rift. Journal of African Earth Sciences 38: 183–197.

Williams MAJ 1966. Age of alluvial clays in the western Gezira, Republic of the Sudan. Nature 211: 270–271.

Williams MAJ 1968. Soil salinity in the west central Gezira, Republic of the Sudan. Soil Science 105(6): 451–464.

Williams MAJ 2009. Late Pleistocene and Holocene environments in the Nile Basin. Global and Planetary Change 69: 1–15.

Williams M 2019. The Nile Basin: Quaternary Geology, Geomorphology and Prehistoric Environments. Cambridge, Cambridge University Press, 405 pp.

Williams M 2020. Water, wind, ice and sea: Prehistoric environments in the Nile Basin between 75,000 and 15,000 years ago. *In:* Leplongeon A, Goder–Goldberger M & Pleurdeau D (Editors)–Not Just a Corridor: Human occupations of the Nile Valley and neighbouring regions between 75,000 and 15,000 years ago. National Museum of Natural History, Paris, pp. 19–37.

Williams MAJ 2021. A river flowing through a desert: late Quaternary environments in the Nile Basin–current understanding and unresolved questions. Journal of Palaeosciences 70: 267–288.

Williams MAJ & Adamson DA 1973. The physiography of the central Sudan. Geographical Journal 139(3): 498–508.

Williams MAJ & Adamson DA 1974. Late Pleistocene desiccation along the White Nile. Nature 248: 584–586.

Williams MAJ & Adamson DA 1980. Late Quaternary depositional history of the Blue and White Nile rivers in central Sudan. *In*: Williams MAJ & Faure H (Editors)–The Sahara and the Nile. Quaternary Environments and Prehistoric Occupation in Northern Africa. Rotterdam, AA Balkema, pp. 281–304.

Williams MAJ & Talbot MR 2009. Late Quaternary environments in the Nile Basin. *In*: Dumont HJ (Editor)–The Nile: Origin, environments, limnology and human use, Monographiae Biologicae 89, Dordrecht, The Netherlands, Springer, pp. 61–72.

Williams MAJ, Adamson DA & Abdulla HH 1982. Landforms and soils of the Gezira: A Quaternary legacy of the Blue and White Nile rivers. *In:* Williams MAJ & Adamson DA (Editors)–A Land between Two Niles: Quaternary geology and biology of the Central Sudan. Balkema, Rotterdam, pp. 111–142.

Williams MAJ, Adamson D, Prescott JR & Williams FM 2003. New light on the age of the White Nile. Geology 31: 1001–1004.

Williams M, Talbot M, Aharon P, Abdl Salaam Y, Williams F & Brendeland KI 2006. Abrupt return of the summer monsoon 15,000 years ago: new supporting evidence from the lower White Nile Valley and Lake Albert. Quaternary Science Reviews 25: 2651–2665.

Williams MAJ, Williams FM, Duller GAT, Munro RN, El Tom OAM, Barrows TT, Macklin M, Woodward J, Talbot MR, Haberlah D & Fluin J 2010. Late Quaternary floods and droughts in the Nile Valley, Sudan: New evidence from optically stimulated luminescence and AMS radiocarbon dating. Quaternary Science Reviews 29: 1116–1137.

Williams MAJ, Duller GAT, Williams FM, Macklin MG, Woodward JC, El Tom OAM, Munro RN, El Hajaz Y & Barrows TT 2015. Causal links between Nile floods and eastern Mediterranean sapropel formation during the past 125 kyr confirmed by OSL and radiocarbon dating of Blue and White Nile sediments. Quaternary Science Reviews 130: 89–108.

Woodward JC, Macklin MG, Krom MD & Williams MAJ 2007. The Nile: Evolution, Quaternary river environments and material fluxes. *In*: Gupta A (Editor)–Large Rivers: Geomorphology and Management. Chichester, John Wiley & Sons, pp. 261–292.

Woodward JC, Macklin MG, Krom MD & Williams MAJ 2022. The Nile: Evolution, Quaternary river environments and material fluxes. *In*: Gupta A (Editor)–Large Rivers. Geomorphology and Management, 2nd revised edition. Chichester, John Wiley & Sons, pp. 388–432.

Woodward J, Macklin M, Fielding L, Millar I, Spencer N, Welsby D & Williams M 2015. Shifting sediment sources in the world's longest river: a strontium isotope record for the Holocene Nile. Quaternary Science Reviews 130: 124–140.